Clathrin-independent endocytosis and retrograde transport in cancer cells promote cytotoxic CD8 T cell activation

Shiqiang XU[1,2], Alix BURIDANT[1], Thibault HIRSCH[3], Massiullah SHAFAQ-ZADAH[4], Estelle DRANSART[4], Benjamin LEDOUX[5], Ludger JOHANNES[4], Pierre VAN DER BRUGGEN[3,6], Pierre MORSOMME[2], Henri-François RENARD[1,5]

Affiliations

[1]UNamur, Namur Research Institute in Life Sciences, Research Unit in Cell Biology, Rue de Bruxelles 61, B-5000, Namur, Belgium.
[2]UCLouvain, Louvain Institute of Biomolecular Science and Technology, Group of Molecular Physiology, Croix du Sud 4-5, B-1348, Louvain-la-Neuve, Belgium.
[3]UCLouvain, de Duve Institute, Avenue Hippocrate 75, B-1200, Bruxelles, Belgium.
[4]Institut Curie, PSL Research University, Cellular and Chemical Biology unit, U1143 INSERM, UMR3666 CNRS, 26 rue d'Ulm, F-75248, Paris Cedex 05, France.
[5]UNamur, Morph-Im Platform, Rue de Bruxelles 61, B-5000, Namur, Belgium.
[6]WELBIO, Belgium.

Correspondence and requests for materials should be addressed to H.F.R. (e-mail: henri-francois.renard@unamur.be)

Abstract

Clathrin-independent endocytosis (CIE) mediates the cellular uptake of endogenous and exogenous cargoes, including bacterial toxins and viruses. Endophilin A3-mediated endocytosis is a specific CIE mechanism that differs from fast endophilin-mediated endocytosis (FEME), with ALCAM and L1CAM being the first confirmed Endophilin A3-specific cargoes. Here, we report ICAM1 as a new Endophilin A3-dependent endocytic cargo. ALCAM and ICAM1 are important components of immune synapses (IS), which are polarized structures formed between immune cells and target cells, such as cancer cells. These molecules transduce essential co-stimulatory signals to T cells to help their effective activation and proliferation. We find that both ALCAM and ICAM1 serve as cargoes for retromer-dependent retrograde transport to the *trans*-Golgi network (TGN) in cancer cells. Interestingly, disrupting Endophilin A3-mediated endocytosis or retromer-dependent retrograde transport machinery impairs activation of autologous cytotoxic CD8 T cells, likely by affecting the polarized redistribution of immune synapse components at the plasma membrane. Altogether, our findings demonstrate that CIE and retrograde transport are key pathways in cancer cells that promote the activation of cytotoxic CD8 T cells.

Introduction

Endocytosis is a physiological process that refers to the membrane bound carrier-mediated internalization of extracellular substances as well as cell membrane components into the cytoplasm of cells. This process is essential for maintaining the homeostasis of cell membrane and regulating signal transduction. Broadly, it can be

divided into conventional clathrin-mediated endocytosis (CME) and unconventional clathrin-independent endocytosis (CIE). While CME has been extensively studied, CIE remains elusive as it includes several distinct mechanisms of endocytosis (Kaksonen & Roux, 2018; Renard & Boucrot, 2021). Upon endocytosis, internalized cargoes merge into early/sorting endosomes, from which they either follow the degradative route towards lysosomes or recycle back to the plasma membrane for a new round of activity. Among the recycled cargoes, some are directly recycled back to the plasma membrane via Rab4/Rab11 recycling endosomes (Sonnichsen *et al*, 2000; van der Sluijs *et al*, 1992). Other cargoes are retrieved from early endosomes by retromer or Commander complexes and further transported to the *trans*-Golgi network (TGN) – a process termed retrograde transport – from where they are finally recycled back to the plasma membrane (Healy *et al*, 2023; McNally *et al*, 2017; Seaman, 2004; Seaman *et al*, 1998). Recently, several lines of evidence have linked retrograde transport to cell polarity maintenance (Shafaq-Zadah *et al*, 2020). For example, $\alpha_5\beta_1$ integrins are transported to the TGN via the retrograde transport route after being endocytosed (Shafaq-Zadah *et al*, 2016). From there, they are re-secreted in a polarized manner to the leading edge of migrating cells, thus maintaining the front-rear polarity, crucial for persistent cell migration (Shafaq-Zadah *et al.*, 2016). In T cells, adaptor molecules Linker for Activation of T cells (LAT) are also transported to the TGN after endocytosis, from which they are re-distributed to the immune synapse (Carpier *et al*, 2018). The immune synapse is a polarized cellular structure formed between immune cells and target cells, *e.g.* between a cytotoxic CD8 T cell and a tumor cell (Dieckmann *et al*, 2016). However, the link between specific unconventional CIE mechanisms and retrograde transport in polarized cellular contexts remains underexplored.

Among the numerous molecular players involved in endocytosis, one can find Endophilin A (EndoA) proteins. EndoA proteins are members of the BAR (Bin/Amphiphysin/Rvs) domain proteins, which are able to sense and/or induce membrane curvature (Gallop *et al*, 2006; Peter *et al*, 2004). There exist three different isoforms of EndoA proteins in mammalian cells, termed EndoA1, A2, and A3 (Micheva *et al*, 1997; Sparks *et al*, 1996). EndoA1 is mainly expressed in brain, and EndoA3 is highly expressed in both brain and testes, while EndoA2 is widely expressed in all tissues (Giachino *et al*, 1997; So *et al*, 2000). Originally, it was reported that EndoAs are mainly involved in CME in neuronal cells, where they recruit dynamins and synaptojanins by binding to the proline-rich domains (PRDs) with their Src-homology 3 (SH3) domains to promote vesicle scission (Ringstad *et al*, 1997; Simpson *et al*, 1999) and clathrin uncoating after scission (Gad *et al*, 2000; Milosevic *et al*, 2011). More recently, EndoAs were reported to play a central role in the clathrin-independent fast endophilin-mediated endocytosis, termed FEME (Boucrot *et al*, 2015). Meanwhile, EndoA2 was reported to function in membrane scission in the clathrin-independent endocytosis of Shiga and cholera toxins (Renard *et al*, 2015; Simunovic *et al*, 2017). It was further reported that the three EndoAs seem to be not totally functionally redundant in CIE, as only EndoA3, but neither A1 nor A2, can specifically mediate the endocytosis of the immunoglobulin (Ig)-like protein ALCAM (Activated Leukocyte Cell Adhesion Molecule). ALCAM is the first identified cargo whose internalization operates in an EndoA3-dependent manner and is driven by extracellular Galectin-8 and glycosphingolipids, in agreement with the glycolipid-lectin (GL-Lect)

endocytosis mechanism (Johannes *et al*, 2016; Lakshminarayan *et al*, 2014; Renard *et al*, 2020). In addition to ALCAM, another Ig-like protein L1 Cell Adhesion Molecule (L1CAM, alternative name CD171) was also confirmed to be a cargo of EndoA3-mediated CIE (Lemaigre *et al*, 2023).

ALCAM, also known as CD166, is an adhesion molecule that is widely expressed in many different types of tissues and overexpressed in several types of cancer, such as bladder, prostate and colorectal carcinomas (Arai *et al*, 2002; Ferragut *et al*, 2021; Weichert *et al*, 2004). It is engaged in cell-cell interactions either by homophilic interactions with other ALCAM molecules (van Kempen *et al*, 2001) or by heterophilic interactions with CD6 (Bowen *et al*, 1995). CD6 is a member of the scavenger receptor cysteine-rich (SRCR) family of proteins that is mainly expressed by immune cells, particularly T lymphocytes, and by some neuronal cells (Aruffo *et al*, 1997; Kamoun *et al*, 1981). Evidence has been shown that heterophilic ALCAM-CD6 interaction is important for immune synapse formation and provides essential co-stimulatory signals for optimal T cell activation and proliferation (Gimferrer *et al*, 2004; Hassan *et al*, 2004; Zimmerman *et al*, 2006). Considering that immune synapse is a polarized cell structure, we wondered whether EndoA3-mediated endocytosis in cancer cells participates in immune synapse formation via retrograde transport of its components, such as ALCAM. Also, given that both ALCAM and L1CAM are Ig-like proteins, we hypothesized that EndoA3-mediated endocytosis could serve as a preferred route for the uptake of Ig-like proteins. Interestingly, another well-known immune synapse component, Intercellular Adhesion Molecule 1 (ICAM1, alternative name CD54), which plays a crucial role in co-stimulating T cell activation by binding to its receptor, Lymphocyte Function-associated Antigen 1 (LFA-1), on the T cell surface, is also an Ig-like protein (Deeths & Mescher, 1999; Van Seventer *et al*, 1990; Zuckerman *et al*, 1998). This led us to investigate whether ICAM1 could be another EndoA3-dependent CIE cargo in cancer cells, and whether its role in forming immune synapses relies on EndoA3-mediated CIE and retrograde transport.

Combining cell biology and immunology experiments, we uncover here that ICAM1 is an EndoA3-dependent endocytic cargo. Moreover, we show that both ALCAM and ICAM1 undergo retromer-dependent retrograde transport to the TGN upon EndoA3-mediated internalization. Disrupting EndoA3-mediated endocytosis or retromer-dependent retrograde transport machinery in cancer cells impairs the activation of autologous cytotoxic CD8 T cells, likely by affecting the polarized redistribution of immune synapse components from the Golgi to the plasma membrane after retrograde transport. Further supporting this hypothesis, disruption of EndoA3-mediated endocytosis in cancer cells impairs efficient recruitment of ICAM1 at the immune synapse and thereby its formation. Hence, our findings highlight the connection between a CIE mechanism and subsequent retrograde transport in a polarized context.

Results

EndoA3-dependent endocytosis mediates internalization of the immune synapse components ALCAM and ICAM1 in cancer cells

To investigate the impact of EndoA3-dependent CIE in cancer cells on the activation of cytotoxic CD8 T lymphocytes, we used the LB33-MEL melanoma cell line, derived from a melanoma patient (LB33) in 1988. This cell line harbours a mutated antigenic peptide encoded by the *MUM3* gene. The MUM-3 peptide is presented on the cell surface by HLA-A*68012 molecules, the HLA-A28 subtype of patient LB33 (Baurain *et al*, 2000; Lehmann *et al*, 1995). An anti-MUM-3-specific CD8 T cell line, obtained from the same patient in 1990 (Lehmann *et al.*, 1995), was used to form immune synapses with LB33-MEL cells *in vitro*. However, LB33-MEL cells do not express detectable amounts of EndoA3 (Renard *et al.*, 2020). For this reason, we generated a stable EndoA3-expressing LB33-MEL cell line. In this cell line, the exogenously expressed EndoA3-GFP protein can be efficiently knocked down by siRNAs targeting EndoA3 (decreased by 80%; Fig EV1A). First, we evaluated colocalization between EndoA3-GFP and ALCAM in this EndoA3-expressing LB33-MEL cell line (LB33-MEL EndoA3+) after a 15 min uptake in the continuous presence of anti-ALCAM antibody in culture medium (Fig 1A). High resolution Airyscan confocal images show a clear colocalization between ALCAM and EndoA3-GFP, confirming that LB33-MEL EndoA3+ cell line can recapitulate the EndoA3-mediated endocytosis of ALCAM (Fig 1A, white arrowheads). Moreover, we quantified the uptake of anti-ALCAM antibody and observed that it was significantly enhanced (3-fold higher) in EndoA3-expressing LB33-MEL cells than in the EndoA3-negative wild-type or empty plasmid transfected stable LB33-MEL cells (Fig 1B, EV1B). A reverse-rescue uptake assay was also conducted in LB33-MEL EndoA3+ cells transfected with EndoA3 siRNAs (Fig 1C, EV1C). Efficiency of siRNAs was confirmed by Western blot analysis (Fig EV1A). ALCAM uptake was significantly decreased by 55% upon EndoA3 depletion (Fig 1C). Taken together, these data demonstrate that EndoA3-expressing LB33-MEL cells can be used to study EndoA3-dependent CIE.

To investigate whether ICAM1 is endocytosed in an EndoA3-dependent manner, similar continuous uptake assays were performed but failed due to the poor quality of commercially available anti-ICAM1 antibodies. Instead, Total Internal Reflection Fluorescence (TIRF) live-cell imaging was used to directly observe the dynamics of EndoA3 and ICAM1 at the plasma membrane of both EndoA3-GFP-expressing HeLa and LB33-MEL cells. Of note, HeLa cells endogenously express EndoA3, while the EndoA3-GFP-expressing HeLa cell line was previously generated and validated by our lab (Lemaigre *et al.*, 2023; Renard *et al.*, 2020). Both HeLa and LB33-MEL cells were transiently transfected with an ICAM1-mScarlet expression plasmid and observed by TIRF live-cell imaging. In both cell lines, EndoA3-GFP formed circular structures around ICAM1 patches (Fig 1D-E, white arrows; Mov EV1-2), and ICAM1 signals gradually disappeared from the plasma membrane (Fig 1D-E; Mov EV1-2). Besides, ICAM1-positive punctate structures could be observed, where EndoA3-GFP was recruited, after which both protein signals subsequently disappeared from the cell surface (Fig 1E, kymograph; Mov EV3), suggesting endocytic events. This is similar to TIRF observations

of the previously identified EndoA3-dependent endocytic cargoes, ALCAM and L1CAM (Lemaigre *et al.*, 2023; Renard *et al.*, 2020). Moreover, it is common to observe EndoA3-GFP positive punctate structures (Fig EV1D, white arrowheads; Mov EV4) or tubular structures (Fig EV1E, white arrowheads; Mov EV5) detaching from the tips or edges of continuously shrinking ICAM1 patches, also suggesting endocytic events. All these observations suggest that ICAM1 is an EndoA3-dependent endocytic cargo.

ALCAM and ICAM1 are cargo clients of retromer-dependent retrograde trafficking

Given the polarized structure of the immune synapse and the previously reported connections between retrograde transport and cell polarity (Carpier *et al.*, 2018; Shafaq-Zadah *et al.*, 2016), we investigated whether ALCAM and ICAM1 are also cargoes for the retrograde transport. To address this question, we used a previously established SNAP-tag-based approach to detect retrograde transport of cargoes from the plasma membrane to the Golgi apparatus (Johannes & Shafaq-Zadah, 2013) (Fig 2A). Briefly, benzylguanine (BG)-labelled cargo-specific antibodies (IgG) are incubated with cells stably expressing the Golgi-resident Galactosyltransferase protein (GalT) fused to GFP and SNAP-tag (GalT-GFP-SNAP). If the cargo follows the retrograde route after endocytosis, it will be delivered to the TGN together with the BG-labelled antibody. Upon arrival in the TGN, BG covalently reacts with the SNAP-tag, generating a large complex (IgG-SNAP-GFP-GalT), trapping the antibody at the TGN. This complex can then be immunopurified and analyzed by Western blot.

Here, we used a HeLa cell line stably expressing the Golgi-resident SNAP-tag construct (HeLa GalT-GFP-SNAP), which has already been validated in previous studies (Shafaq-Zadah *et al*, 2021; Shafaq-Zadah *et al.*, 2016). We also generated a LB33-MEL cell line stably expressing the same Golgi-resident SNAP-tag construct (LB33-MEL GalT-GFP-SNAP, Fig EV2A-B). First, we validated the functionality of the SNAP-tag in both cell lines using the SNAP-Cell® TMR-Star reagent (Fig 2B for HeLa; Fig EV2A for LB33-MEL). We observed a strong and specific colocalization of TMR-Star with the GFP signal of the SNAP-tag constructs in both cell lines. Second, immunofluorescence experiments showed that the SNAP-tag construct co-distributes with the *TGN*-specific marker TGN46 in LB33-MEL cells, thus confirming the correct and specific localization of the construct (Fig EV2B).

Next, we used both cell lines in retrograde transport assays. BG-labelled anti-ALCAM or anti-ICAM1 antibodies were added to the cell culture medium for a 4-hour continuous uptake. If ALCAM or ICAM1 are retrograde cargoes, their specific BG-tagged antibodies (BG-IgGs) should also move along into the Golgi compartment and produce covalently bound IgG-SNAP-GFP-GalT complex species (simplified as SNAP signal) that should be observed in Western blot. Interestingly, we found that both ALCAM and ICAM1 are retrograde transport cargoes in HeLa cells, as the IgG-SNAP-GFP-GalT complexes were indeed detected by Western blotting when both BG-labelled antibodies were used (band ~ 210 kDa, Fig 2C-D, IB: anti-SNAP). As negative controls, we used unlabelled antibodies (IgGs), and no bands were observed (Fig 2C-D). In addition, we depleted EndoA3 by RNA interference in HeLa cells (Fig 2C-D, EV2E), causing a significant decrease of the

IgG-SNAP signal intensity (decreased by 60% for ALCAM and 64% for ICAM1, Fig 2C-D). We also carried out retrograde transport assays with BG-labelled anti-ALCAM antibodies in the SNAP-tag expressing LB33-MEL cell line (Fig EV2C). As this cell line was generated from the wild-type LB33-MEL background which does not express detectable levels of EndoA3, we transfected it transiently with an EndoA3-GFP expression plasmid. Interestingly, we observed that the SNAP signal was ~50% higher upon EndoA3-GFP expression, as compared to the control condition where cells were transiently transfected with a plasmid allowing free GFP expression (Fig EV2C). Altogether, these data confirm that both ALCAM and ICAM1 are EndoA3-dependent endocytic cargoes, and further demonstrate that both proteins are retrograde transport cargoes, trafficking from the plasma membrane to the Golgi apparatus.

Subsequently, we wondered if these two retrograde transport cargoes need the canonical retromer complex machinery for endosomal sorting and retrograde transport to the TGN. The retromer complex is for now the best-studied retrograde transport sorting machinery and is composed of three subunits in mammalian cells, which are VPS26, VPS29 and VPS35 (Hierro *et al*, 2007; Seaman, 2004). Two paralogues of VPS26 subunit exist: VPS26A, which is highly expressed in basically all tissues, and VPS26B, which is mainly enriched in the brain (Bugarcic *et al*, 2011; Kerr *et al*, 2005). To address the role of retromer in the retrograde trafficking of ALCAM and ICAM1, we carried out SNAP-tag-based retrograde transport assays in HeLa cells where VPS35 and VPS26A were knocked down by RNA interference (Fig 2E-F, EV2F). In cells treated with negative control siRNA, unlabelled antibodies led to no detectable SNAP signal in Western blot (Fig 2E), while BG-labelled antibodies showed a clear one (Fig 2E-F), which is consistent with our previous experiments. Interestingly, depletion of either VPS35 or VPS26A caused a significant reduction of SNAP signal intensity for both cargoes (Fig 2E-F). Similar results were also obtained for ICAM1 in SNAP-tag expressing LB33-MEL cells, even though EndoA3 is not detectably expressed in these cells (Fig EV2D and EV2G). This suggests the existence of alternative endocytic mechanisms for this cargo, which result, at least partially, in its retrograde transport to the Golgi. Taken together, these data further demonstrate that the retrograde transport of significant fractions of ALCAM and ICAM1 to the Golgi is mediated by the retromer complex.

Inhibition of both EndoA3-dependent endocytosis and retromer-mediated retrograde transport impairs cytotoxic CD8 T cell activation

Based on our results shown before and considering that ALCAM and ICAM1 are key components of the immune synapses, we hypothesized that their clathrin-independent endocytosis and subsequent retrograde transport might influence CD8 T cell activation. To test this, we conducted CD8 T cell stimulation assays using LB33-MEL cells, with and without EndoA3 expression. EndoA3-expressing LB33-MEL cells were treated with either control or EndoA3-targeting siRNAs before being co-cultured with CD8 T cells. The cells were then analyzed by flow cytometry to assess intracellular cytokine production in T cells (Fig 3A). Interestingly, when CD8 T cells were stimulated with EndoA3-depleted LB33-MEL cells, both the percentage of T cells producing interleukin-2 (IL-2) and tumor necrosis factor α (TNFα) (Fig 3B, upper and middle panels) and the absolute amounts of

these cytokines (Fig 3C, upper and middle panels) significantly decreased compared to CD8 T cells stimulated with EndoA3-expressing LB33-MEL cells. Although the percentage of T cells producing interferon γ (IFNγ) remained unchanged (Fig 3B, bottom panel), the absolute amount of IFNγ produced was still significantly reduced (Fig 3C, bottom panel).

Next, we performed IFNγ secretion assays, where CD8 T lymphocytes were stimulated with differentially treated LB33-MEL cells, after which the supernatant was analyzed by enzyme-linked immunosorbent assay (ELISA) (Fig 3D). Wild-type, empty plasmid control, and EndoA3-GFP-expressing LB33-MEL cells all stimulated CD8 T cells to secrete IFNγ, as compared to the control condition where T cells were kept alone (Fig 3E). EndoA3-expressing LB33-MEL cells significantly enhanced CD8 T cell activation, with T cells secreting approximately 70% more IFNγ compared to wild-type or empty plasmid conditions (Fig 3E). This effect was lost when EndoA3 was depleted from LB33-MEL cells using RNA interference (Fig 3E). The efficiency of EndoA3-GFP depletion was confirmed by flow cytometry (Fig EV3A). We hypothesized that EndoA3-mediated CIE in cancer cells may influence retrograde transport and the subsequent polarized redistribution of immune synapse components, such as ALCAM and ICAM1, thereby affecting T cell activation. To explore this, we assessed the impact of disrupting the retromer complex in cancer cells on CD8 T cell activation. We first depleted the retromer subunits VPS26A and VPS35 using RNA interference in EndoA3-expressing LB33-MEL cells and then examined the effects on CD8 T cell activation by measuring IFNγ secretion. While VPS35 depletion showed no significant effect, depleting VPS26A clearly impaired CD8 T cell activation (Fig 3F, EV3B).

To conclude, these data suggest that inhibition of EndoA3-dependent endocytosis in cancer cells impairs CD8 T cell activation by affecting the retrograde transport of immune synapse components, such as ALCAM and ICAM1. This likely prevents the efficient recruitment of these components to participate in immune synapse formation through polarized re-distribution from the TGN.

Inhibition of EndoA3-dependent endocytosis affects ICAM1 recruitment to the vicinity of CD8 T cells

The disruption of EndoA3-dependent endocytosis impairs CD8 T cell activation possibly through impaired polarized re-distribution of immune synapse components to the plasma membrane. To verify this possibility, we monitored the recruitment of ICAM1 to the immune synapse with high resolution Airyscan confocal microscopy, as the importance of ICAM1 for T cell activation is already well-established (Van Seventer *et al.*, 1990). Although we could successfully get LB33-MEL cells transiently transfected with ICAM1-expressing plasmid (Fig 1E), the transfection efficiency was very low, thereby limiting the possibility of using LB33-MEL cells for immune synapse imaging. To address this issue, we generated a stable HLA-A*68012-expressing HeLa cell line. Wild-type HeLa cells lack HLA-A*68012, making them unable to present MUM-3 antigenic peptide to stimulate CD8 T cell activation (Fig EV4A). When exogenous MUM-3 peptide was added to HLA-A*68012-expressing HeLa cells, they successfully stimulated the anti-MUM-3 CD8 T cells

to secrete IFNγ (Fig EV4A), as well as to proliferate (Fig EV4B). Thereby, these data together confirmed the functionality of this HLA-A*68012-expressing HeLa cell line.

To monitor the recruitment of ICAM1 to the immune synapse, HLA-A*68012-expressing HeLa cells transiently expressing GFP-tagged ICAM1 were loaded with the MUM-3 peptide and co-cultured with CD8 T cells. Using Airyscan live-cell imaging, we were able to observe ICAM1-containing vesicular structures moving from inside the cells towards the contact area with CD8 T cells and then fusing with it (Fig 4A, white arrowheads; Mov EV6). Moreover, in immunofluorescence experiments using HeLa cells transiently expressing ICAM1-mScarlet, we observed a strong accumulation of ICAM1 signal in the contact zone with CD8 T cells (Fig 4B, EV4C, white arrowheads). Next, we treated ICAM1-mScarlet-expressing HeLa cells with control or EndoA3 siRNAs and incubated them with CD8 T cells (Fig 4C, EV4D). For quantification purposes, this experiment was conducted on cells in suspension where they adopt a regular spherical shape, which are easier to segment by quantification algorithms (Fig 4C, EV4D, phalloidin channel). The ICAM1 recruitment ratio in the vicinity of T cells was measured (see Materials and Methods). Surprisingly, on T cells, the ICAM1 signal was not limited to the contact region of the conjugates, but often expanded to surround the whole T cell (Fig 4C, EV4D). Quantifications revealed that depletion of EndoA3 in HLA-A*68012-expressing HeLa cells induced a slight but significant decrease of ICAM1 recruitment to the vicinity of anti-MUM-3 CD8 T cells (Fig 4D), which aligns with the previously observed impaired T cell activation (Fig 3).

Altogether, these observations suggest that EndoA3-mediated CIE in cancer cells promotes the recruitment of components to the immune synapse, likely by polarized trafficking from the Golgi to the plasma membrane in contact with the T cell.

CD8 T cells compensate the decreased recruitment of immune synapse components by increasing the size of immune synapses

Lastly, we explored the consequences of EndoA3 or VPS26A inhibition in cancer cells on the morphology of immune synapses. To study this, we imaged immune synapses formed between anti-MUM-3 CD8 T cells and EndoA3-expressing LB33-MEL cells in suspension with Airyscan confocal microscopy (Fig 5A and 5D, EV5A-B). We observed that immune synapses formed between CD8 T cells and EndoA3- or VPS26A-depleted LB33-MEL cells appeared to be larger than those formed between CD8 T cells and control LB33-MEL cells. Quantifications of the size of each immune synapse confirmed this observation, showing that the immune synapses are 24% and 12% larger following the depletion of EndoA3 and VPS26A, respectively (Fig 5B and 5E). The efficiency of siRNA was also validated by Western blot analyses (Fig 5C and 5F). Taken together, these data suggest that CD8 T cells try to compensate the decreased recruitment of the immune synapse components – due to inhibition of CIE or retrograde transport in cancer cells – by increasing the size of the immune synapses. However, despite their larger size, these immune synapses fail to promote CD8 T cell activation effectively (Fig 3, EV3).

In summary, disruption of endoA3-mediated CIE and subsequent retrograde transport in cancer cells hinders the recruitment of immune synapse components, such as ALCAM and ICAM1, likely through polarized re-distribution from the TGN to participate in immune synapse formation with autologous CD8 T cells. Consequently, this leads to decreased co-stimulatory signals necessary for effective CD8 T cell activation. Although T cells attempt to compensate for the decreased co-stimulatory signals by expanding their contact area with tumor cells, this compensation is insufficient, ultimately resulting in their impaired activation (Fig 6).

Discussion

In this study, we discovered that ICAM1 is a new cargo of EndoA3-mediated CIE, thus extending the list of previously reported cargoes, the cell surface Ig-like proteins ALCAM and L1CAM (Lemaigre *et al.*, 2023; Renard *et al.*, 2020). Surprisingly, in the first paper of *Boucrot et al.* (2015) reporting the existence of FEME, the internalization of ICAM1 was not affected when all the three EndoA isoforms were depleted. This discrepancy could be explained by the different cell lines used: *Boucrot et al.* (2015) used a human T cell line (Kit255), where EndoA3 might be poorly expressed (Giachino *et al.*, 1997; Kjaerulff *et al*, 2011), whereas we used human cancer cell lines (a HeLa cell line with endogenous EndoA3 expression and a melanoma cell line LB33-MEL engineered to stably express EndoA3). In addition, a recent consensus is that FEME is mostly mediated by EndoA2 isoform (Renard & Boucrot, 2021). Hence, our data further support the idea that the different EndoA isoforms are not totally functionally redundant and that EndoA3 mediates an unconventional endocytic modality distinct from FEME, as proposed in a previous study of our lab (Renard *et al.*, 2020).

Interestingly, all three confirmed EndoA3-dependent endocytic cargoes – ALCAM, L1CAM and ICAM1 – are Ig-like cell adhesion molecules. This indicates that there might exist a cargo recognition pattern for EndoA3-mediated CIE. Unlike CME, where membrane cargoes are recognized by adaptor proteins binding to specific identified sorting signals present in the cytosolic tails of the cargoes (Traub & Bonifacino, 2013), the mechanisms for cargo recognition in CIE are emerging only now (Lakshminarayan *et al.*, 2014; Moreno-Layseca *et al*, 2021). In FEME, it is believed that EndoA proteins can either directly sort out G protein-coupled receptors (GPCRs) for endocytosis by binding to PRDs in GPCRs with their SH3 domains (Boucrot *et al.*, 2015; Tang *et al*, 1999), or indirectly sort out endocytic cargoes by binding to other proteins, such as binding to CIN85 for sorting out EGFR and HGFR (Petrelli *et al*, 2002; Soubeyran *et al*, 2002), and binding to srGAP1 for sorting out ROBO1 (Genet *et al*, 2019). However, how EndoA3-dependent endocytic cargoes are recognized and sorted remains unclear. Previous studies from our lab have shown that the cytosolic tails of ALCAM and L1CAM physically interact with EndoA3, but not EndoA2 (Lemaigre *et al.*, 2023; Renard *et al.*, 2020). However, specific interaction motifs have not been identified in those two cargoes, yet. It also remains unknown whether the interaction with EndoA3 is direct or indirect, and, if direct, which part of EndoA3 protein is responsible for this interaction. Nevertheless, accumulating evidence showing that Ig-like cell adhesion molecules are preferential EndoA3-

dependent cargoes suggest that a shared common recognition pattern might exist in this cargo superfamily, which deserves further investigations.

In addition, we found that two of the three confirmed EndoA3-dependent endocytic cargoes, ALCAM and ICAM1, are also retromer-dependent retrograde transport cargoes. The fact that ICAM1 is a retromer-dependent retrograde transport cargo aligns with previously published proteomic analysis of retromer-dependent cargoes, where ICAM1 was one of the hits (Steinberg *et al*, 2013). Although the link between retrograde transport and cell polarity has been previously established (Carpier *et al.*, 2018; Shafaq-Zadah *et al.*, 2020; Shafaq-Zadah *et al.*, 2016), the relationship between CIE and subsequent retrograde transport in polarized cellular contexts is largely unknown. Here, we propose that EndoA3-dependent endocytic cargoes follow the retrograde transport route, thus connecting this specific CIE to polarized conditions.

The retromer complex is one of the two complexes that can retrieve cargoes from endosomes for retrograde transport. The other one is Commander complex, which is composed of the CCC and retriever complexes. The CCC complex comprises two coiled coil domain-containing proteins CCDC22 and CCDC93, ten COMMD (copper metabolism MURR1 (Mouse U2af1-rs1 region 1) domain) family members COMMD1-COMMD10, and DENND10 (differentially expressed in normal and neoplastic cells-containing protein 10, also called FAM45A) (Healy *et al.*, 2023; Mallam & Marcotte, 2017; Singla *et al*, 2019; Wan *et al*, 2015). The retriever complex is structurally similar to the retromer complex and is composed of C16orf62 (VPS35L), DSCR3 (VPS26C), and VPS29 (Chen *et al*, 2019; McNally *et al.*, 2017). Generally, Commander is considered as a complex for retromer-independent endosomal cargo sorting for retrograde transport, though many cargoes can use both complexes (McNally *et al.*, 2017). In our study, we confirmed that both ALCAM and ICAM1 are retromer-dependent retrograde transport cargoes. However, even though the depletion of the retromer subunits VPS35 and VPS26A both impaired the retrograde transport of ALCAM and ICAM1 in HeLa cells, the effect of VPS26A depletion was systematically stronger than that caused by the loss of VPS35 (Fig 2E, F). Moreover, only the depletion of the retromer subunit VPS26A impaired the activation of CD8 T cells, while VPS35 depletion did not have any significant effect (Fig 3F). Western blot analyses showed that the treatment with VPS35 siRNAs causes a significant loss of VPS26A, while the treatment with VPS26A siRNAs induces a milder loss of VPS35 (Fig 2E, F, EV2D, 2F and 2G). Interestingly, it was previously reported that the depletion of VPS35 or VPS29 accompanies the degradation of other subunits, whereas depletion of VPS26A had no effect on VPS29 and VPS35 levels. Hence, the authors suggested that VPS29 and VPS35 form a biologically stable sub-complex *in vivo* (Fuse *et al*, 2015). Our results partially align with their discoveries as the depletion of VPS26A causes milder decrease of VPS35 signal. Still, based on these observations, we hypothesize that there may exist a mutual compensatory effect between the retromer and Commander complexes for some cargoes. Depletion of VPS35 in HeLa cells caused almost complete loss of the retromer complex, which might trigger the compensation by the Commander complex for retrograde transport. However, depletion of VPS26A still preserves the VPS29-VPS35 intermediate of retromer complex (Fuse *et al.*, 2015), which might inhibit the compensatory effect by the Commander complex via mechanisms remaining to be

discovered. This could explain why, in our data, depletion of VPS35 caused a milder effect on the retrograde transport of ALCAM and ICAM1 in HeLa cells and why it did not significantly affect CD8 T cell activation. As to why, in GalT-GFP-SNAP-expressing LB33-MEL cells, the depletion of VPS35 and VPS26A caused similar effects on the retrograde transport of ICAM1 (Fig EV2D), we hypothesize that it could be because this LB33-MEL cell line does not express detectable endogenous levels of EndoA3, hence leading to much less efficient ICAM1 uptake and lower impact of compensation phenomena by the Commander complex. Overall, future investigations on potential mutual compensation between the retromer and Commander complexes in the retrograde transport of Ig-like proteins are necessary.

To conclude, in this study, we identified a new EndoA3-dependent endocytic cargo ICAM1, which, along with the previously identified EndoA3-depedent cargo ALCAM, is a retromer-dependent retrograde transport cargo. Both ALCAM and ICAM1 are immune synapse components. The disruption of EndoA3-mediated endocytosis and retromer-dependent retrograde transport in cancer cells impairs the activation of CD8 T cells, possibly by affecting the recruitment of these immune synapse components through retrograde transport and subsequent polarized redistribution to plasma membrane. Hence, our study establishes a potential link between specific CIE and cell polarity formation via retrograde transport. Furthermore, our results may be relevant in pathophysiological contexts, where protein trafficking pathways could be modulated to tune the recognition and elimination of cancer cells by the immune system. The use of protein trafficking mechanisms as therapeutic targets appears as an exciting possibility, which certainly deserves to be addressed in future studies.

Figures & Legends

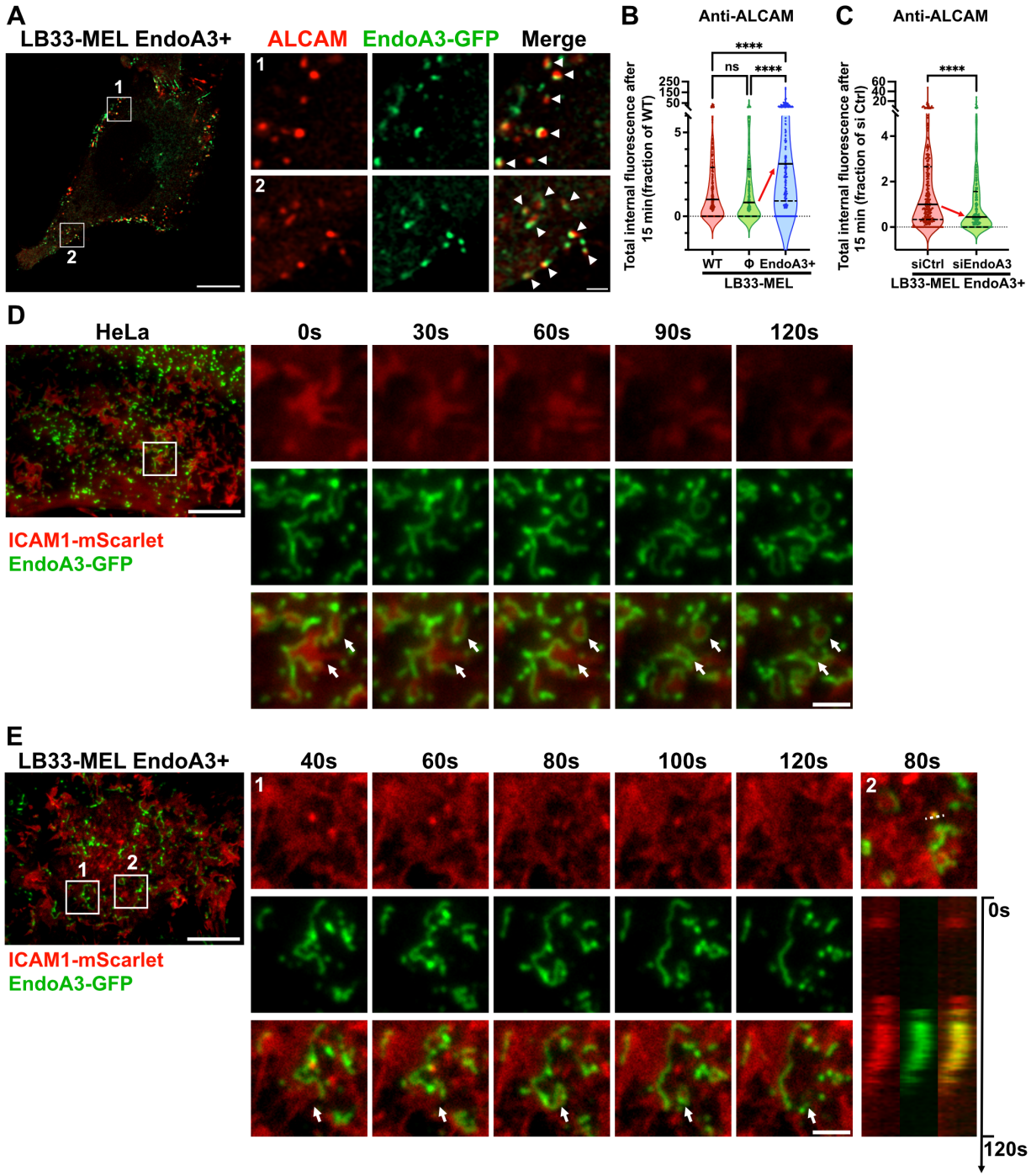

Figure 1. EndoA3-dependent CIE mediates the uptake of immune synapse components ALCAM and ICAM1 in cancer cells.

A-C Continuous uptake of anti-ALCAM antibody for 15 min at 37°C in the following LB33-MEL cell lines: wild-type (WT, B), stably transfected with empty plasmid (Φ, B), or stably expressing EndoA3-GFP (LB33-MEL EndoA3+, A-C). In (C), cells were transfected with siRNAs: negative control (siCtrl) or against EndoA3

(siEndoA3). Quantification of EndoA3 depletion by western blots in Fig EV1A. (A) Airyscan images of Anti-ALCAM (red) and EndoA3-GFP (green). White arrowheads show colocalization between ALCAM and EndoA3. Scale bars: 10 µm (full size image), 1 µm (enlarged cropped areas). (B-C) Quantifications of anti-ALCAM internalization, expressed as fractions of WT condition (B) or siCtrl condition (C). (B) n cells: WT, n = 270; Φ, n = 279; EndoA3+, n = 274. (C) n cells: siCtrl, n = 350; siEndoA3, n = 234. Representative image examples in Fig EV1B-C.

D-E Live-cell TIRF images of EndoA3-GFP (stable) and ICAM1-mScarlet (transient) in HeLa (D) and LB33-MEL (E) cells. Time series show enlarged cropped areas extracted from Mov EV1 (D) and Mov EV2 (E). White arrows indicate dynamic co-distribution of both signals. Kymograph in (E) was made along dashed line region in the 2nd cropped area (D; Mov EV3). Scale bars: 10 µm (full size image), 2 µm (enlarged cropped areas).

Data information: All images (A, D and E) are representative of two independent experiments. In (B-C), data are pooled from three independent experiments. Data are presented as median and quartiles. ns, not significant. ****P < 0.0001 (B, Kruskal-Wallis test with Dunn's multiple comparison test; C, Mann-Whitney test). Source data are available online for this figure.

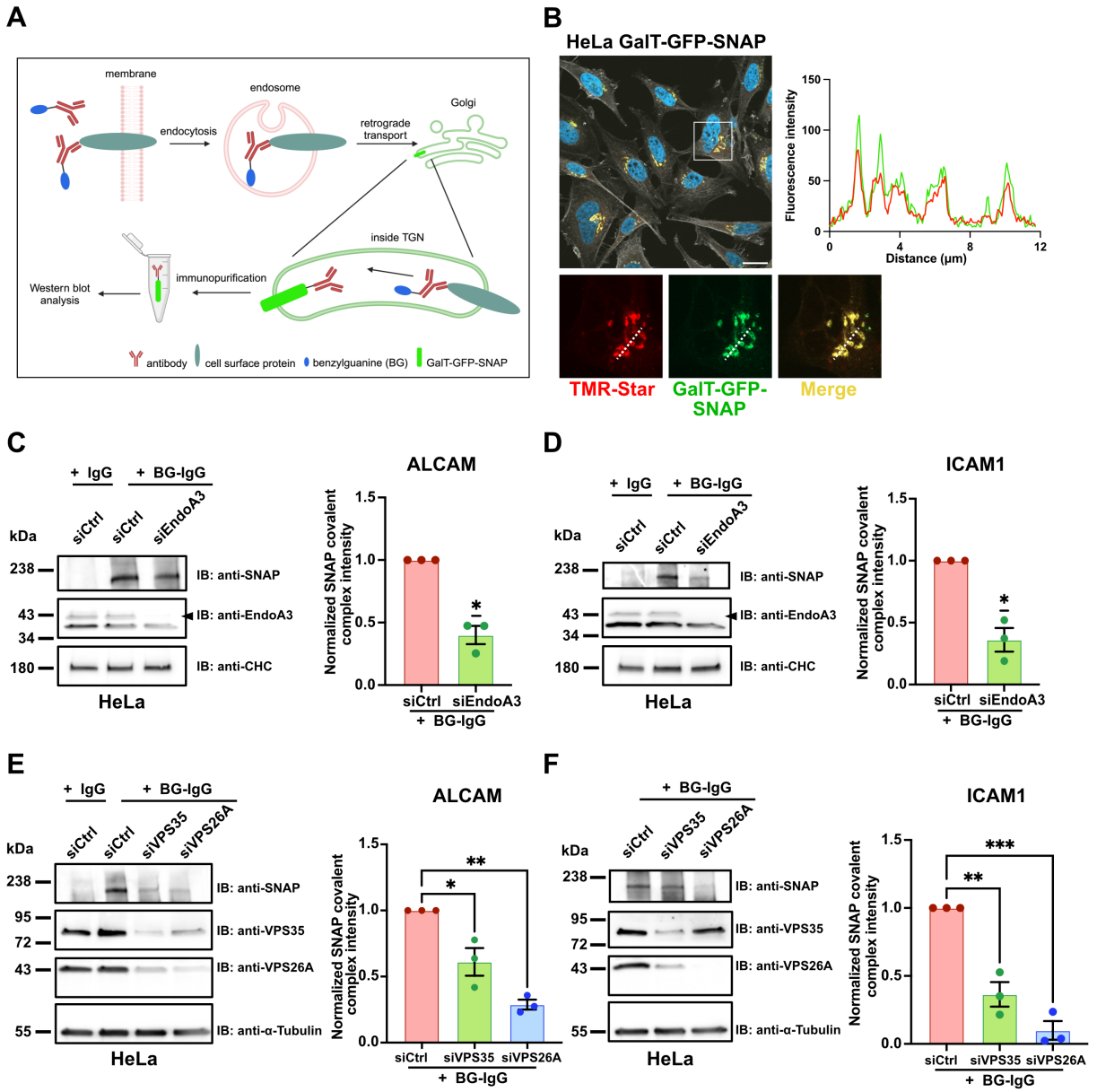

Figure 2. Immune synapse components ALCAM and ICAM1 are retrograde transport cargoes that rely on retromer

A Illustration of the SNAP-tag-based BG-labelled antibody uptake assay to study membrane protein endocytosis and retrograde transport.

B Confocal images of GalT-GFP-SNAP (green) and TMR-Star (red) in HeLa cells stably expressing the Golgi-resident GFP-fused SNAP-tag construct (HeLa GalT-GFP-SNAP). Actin (phalloidin, white) and nuclei (DAPI, blue) were also stained. Fluorescence intensity profile was made along the dashed line region in enlarged cropped area, and shows the colocalization of both signals. Scale bar: 20 µm.

C-F Retrograde transport of ALCAM and ICAM-1. Continuous BG-labelled anti-ALCAM (C and E) and anti-ICAM1 (D and F) antibody uptake for 4h at 37°C in HeLa GalT-GFP-SNAP cells. (C-D) Western blot analysis of HeLa GalT-GFP-

SNAP cells transfected for 72h with siRNAs: negative control (siCtrl) or against EndoA3 (siEndoA3). Immunodetection made with anti-SNAP, anti-EndoA3 and anti-clathrin heavy chain (CHC, loading control) antibodies. Quantification of the covalent IgG-SNAP-GFP-GalT complex (IB:anti-SNAP) is shown as fractions of siCtrl condition (histogram). Quantification of EndoA3 depletion is shown in Fig EV2E. (E-F) Western blot analysis of HeLa GalT-GFP-SNAP cells transfected for 72h with siRNAs: negative control (siCtrl) or against retromer subunits (siVPS35 and siVPS26A). Immunodetection made with anti-SNAP, anti-VPS35, anti-VPS26A and anti-α-Tubulin (loading control) antibodies. Quantification of the covalent IgG-SNAP-GFP-GalT complex is shown as fractions of siCtrl condition (histogram). Quantification of VPS35 and VPS26A depletion is shown in Fig EV2F.

Data information: In (B), images are from a single experiment. Quantification data (C-F) are pooled from three independent experiments. Data are presented as mean ± SEM. *P < 0.05, **P < 0.01, ***P < 0.001 (C-D, one sample *t* test; E-F, RM one-way ANOVA with Dunnett's multiple comparison test). Source data are available online for this figure.

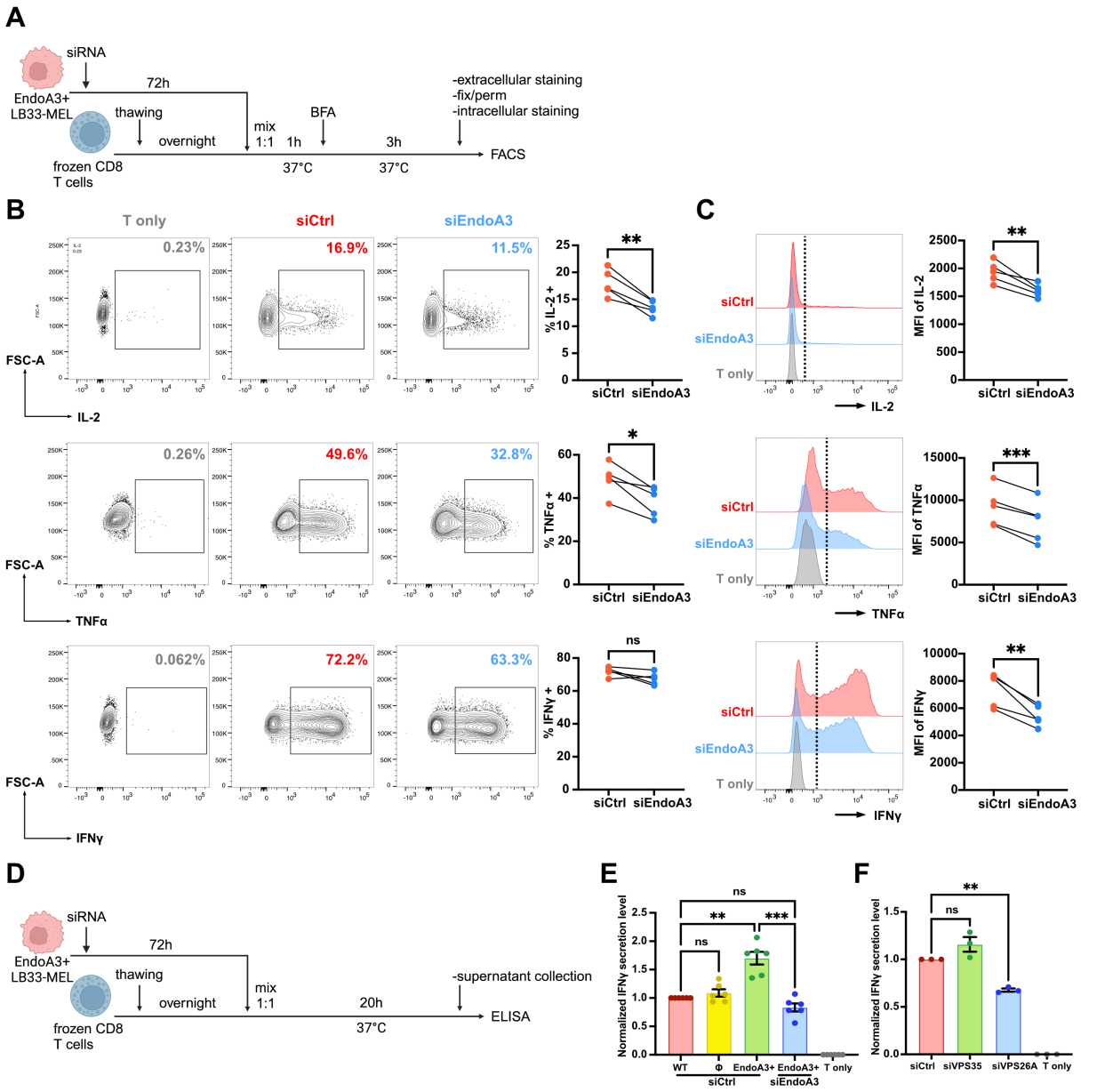

Figure 3. Inhibition of EndoA3-dependent endocytosis and retrograde transport impairs T cell activation

A Scheme of flow cytometry analysis of cytokine production inside CD8 T cells stimulated by siRNA transfected EndoA3+ LB33-MEL cells.

B-C Flow cytometry analysis of CD8 T cell intracellular cytokine production after co-culture for 4h at 37°C with: no LB33-MEL (T only), EndoA3+ LB33-MEL transfected with negative control siRNA (siCtrl) or with siRNA against EndoA3 (siEndoA3). Quantification of EndoA3 depletion is shown in Fig EV3A. (B) Representative examples and quantifications (scatter plots) of the percentages of cytokine producing CD8 T cells (up, IL-2; middle, TNFα; bottom, IFNγ) after being stimulated by siCtrl or siEndoA3 treated LB33-MEL EndoA3+ cells. (C) Representative examples and quantifications (scatter plots) of the absolute

amount of cytokines produced by CD8 T cells (up, IL-2; middle, TNFα; bottom, IFNγ; presented as median fluorescence intensity, MFI) after stimulation by siCtrl or siEndoA3 treated LB33-MEL EndoA3+ cells.

D Scheme of ELISA analysis of cytokine secretion from CD8 T cells stimulated with siRNA transfected EndoA3+ LB33-MEL cells.

E Quantification of IFNγ secretion (detected by ELISA) from CD8 T cells, cultured alone (T only) or co-cultured for 20h with the following LB33-MEL cell lines: wild-type LB33-MEL cells (WT), LB33-MEL cells stably transfected with empty (Φ) or EndoA3-GFP encoding plasmid (EndoA3+), treated with negative control siRNA (siCtrl) or with EndoA3-targeting siRNA (siEndoA3). Data are presented as fractions of WT siCtrl condition. The absolute concentration of secreted IFNγ in the supernatant of WT siCtrl condition is 2203 ± 201 (mean ± SEM) pg/mL.

F Quantification of IFNγ secretion (detected by ELISA) from CD8 T cells, cultured alone (T only) or co-cultured for 20h at 37°C with EndoA3+ LB33-MEL cells transfected with siRNAs: negative control (siCtrl), or against retromer subunits (siVPS35 or siVPS26A). Data are presented as fractions of siCtrl condition. The absolute concentration of secreted IFNγ in the supernatant of siCtrl condition is 4077 ± 99.62 (mean ± SEM) pg/mL. Quantification of VPS35 and VPS26A depletion is shown in Fig EV3B.

Data information: In (B-C), data are pooled from five independent experiments. In (E), data are pooled from six independent experiments. In (F), data are pooled from three independent experiments. In (E-F), data are presented as mean ± SEM. ns, not significant. *P < 0.05, **P < 0.01, ***P < 0.001 (B-C, paired *t* test; E, RM one-way ANOVA with Tukey's multiple comparison test; F, RM one-way ANOVA with Dunnett's multiple comparison test). Source data are available online for this figure.

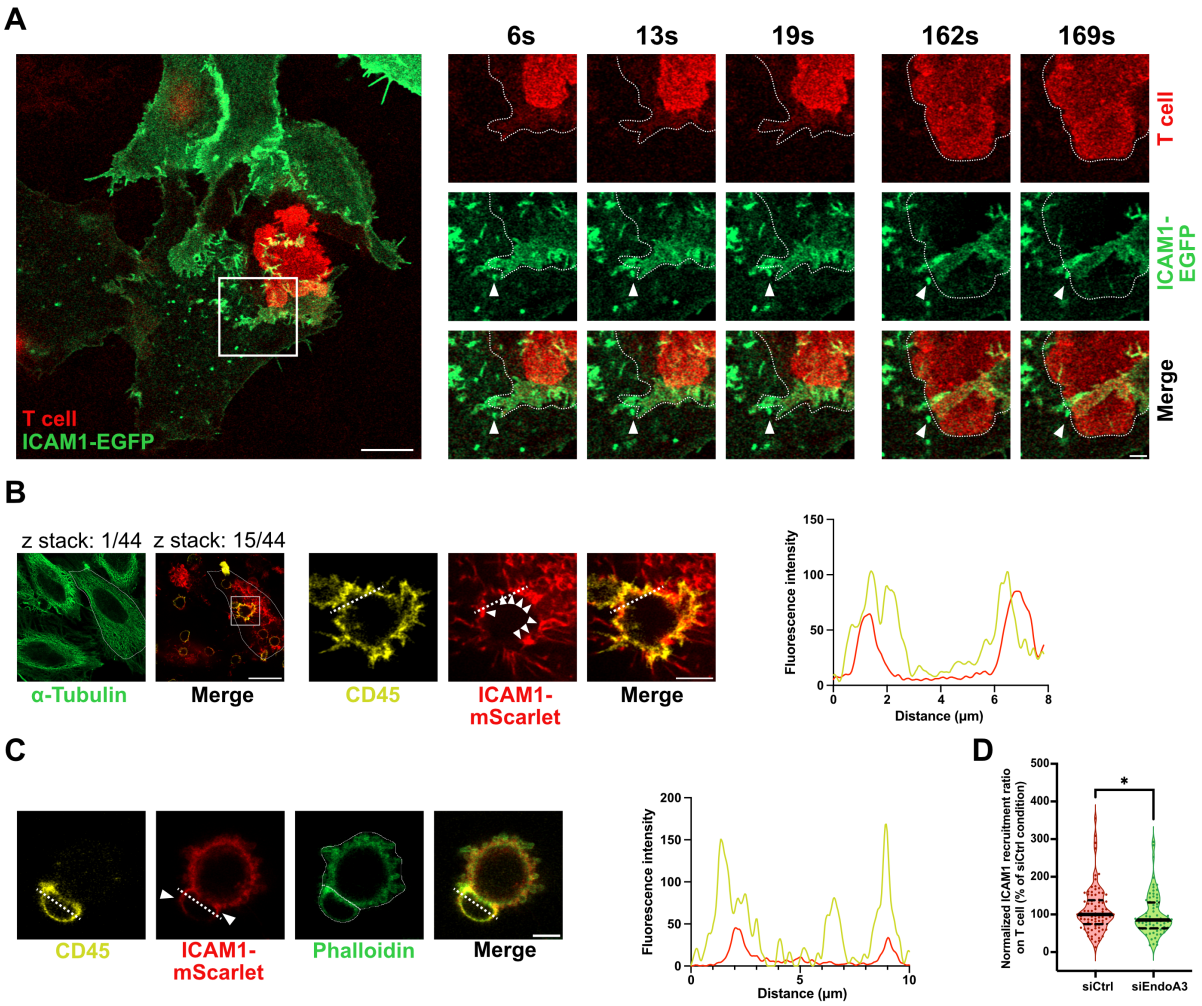

Figure 4. Inhibition of EndoA3-mediated CIE affects ICAM1 recruitment to immune synapses

A Live-cell Airyscan images of an IS-like conjugate formed between a CD8 T cell (red) and an adherent stable HLA-A*68012-expressing HeLa cell line transiently expressing ICAM1-EGFP (green). Time series show enlarged cropped areas extracted from Mov EV6. The dashed line contours delineate the contact area between the HeLa cell and the CD8 T cell. White arrowheads show two ICAM1-positive vesicular structures moving towards the contact area. Scale bars: 10 μm (full size image), 2 μm (enlarged cropped areas).

B Airyscan images of an IS-like conjugate formed between a CD8 T cell (stained for CD45, yellow) and an adherent stable HLA-A*68012-expressing HeLa cell (stained for microtubules, green) transiently expressing ICAM1-mScarlet (red). White arrowheads indicate recruitment of ICAM1 to the vicinity of CD8 T cell. The fluorescence intensity profile was made along the dashed line region in the enlarged cropped area, and shows enrichment of ICAM1 signal close to the CD8 T cell surface. Scale bars: 20 μm (full size image), 5 μm (enlarged cropped areas).

C Airyscan images of an IS-like conjugate formed between a CD8 T cell (stained for CD45, yellow) and a stable HLA-A*68012-expressing HeLa cell (stained for

actins, green) transiently expressing ICAM1-mScarlet (red) in suspension. The fluorescence intensity profile was made along the dashed line region. Cell segmentation (white contour) was based on the actin staining for further quantifications (D). Scale bar: 5 µm.

D Quantification of relative ICAM1 recruitment to the vicinity of CD8 T cell when an IS-like conjugate is formed between a CD8 T cell and a stable HLA-A*68012-expressing HeLa cell transiently expressing ICAM1-mScarlet in suspension. HLA-A*68012-expressing HeLa cells were transfected for 72h with siRNAs: negative control (siCtrl) or against EndoA3 (siEndoA3). Western blot analysis of EndoA3 depletion is shown in Fig EV4E. n conjuagates: siCtrl, n = 85; siEndoA3, n = 75.

Data information: In (A) and (C), images are representative of three independent experiments. In (B), images are from a single experiment. In (D), data are pooled from three independent experiments. Data are presented as median and quartiles. *P < 0.05 (Kolmogorov-Smirnov test). Source data are available online for this figure.

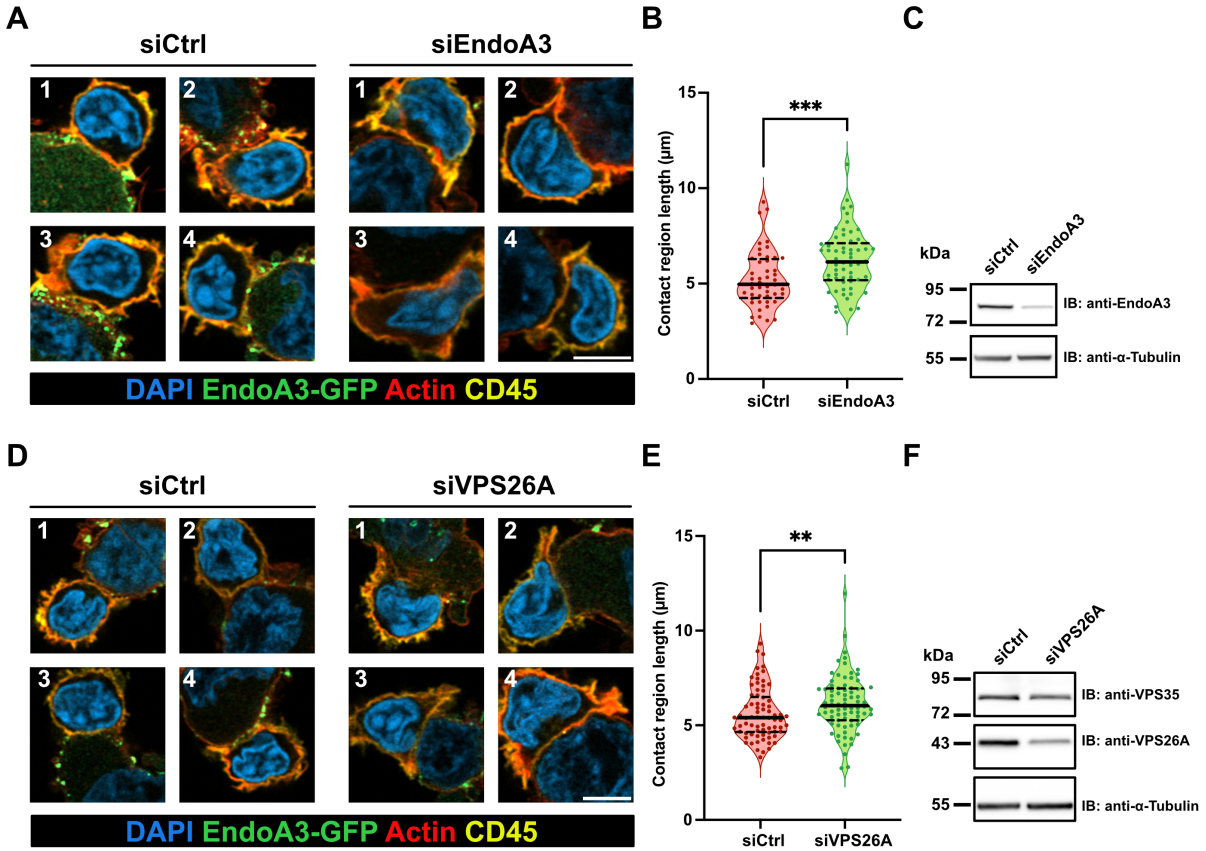

Figure 5. Inhibition of EndoA3-mediated CIE and retrograde transport affects immune synapse morphology

A, D Airyscan images of IS-like conjugates formed between CD8 T cells (stained for CD45, yellow) and stable EndoA3-GFP-expressing LB33-MEL cells (EndoA3-GFP, green) transfected for 72h with different siRNAs: negative control (siCtrl), siRNAs against EndoA3 (siEndoA3, A) or against VPS26A (siVPS26A, D). Actin (phalloidin, red) and nuclei (DAPI, blue) were also stained. Four examples are displayed per condition. Scale bar: 5 µm.

B, E Quantifications of the sizes of IS-like conjugates formed between CD8 T cells and stable EndoA3-GFP-expressing LB33-MEL cells transfected with different siRNAs from images in panels A and D. (B) n conjugates: siCtrl, n = 48; siEndoA3, n = 58. (E) n conjugates: siCtrl, n = 74; siVPS26A, n = 78.

C, F Western blot analyses of stable EndoA3-GFP-expressing LB33-MEL cells transfected with siRNAs: negative control (siCtrl), siRNAs against EndoA3 (siEndoA3, C) or against VPS26A (siVPS26A, F). In (C), immunodetection was made with an anti-EndoA3 antibody. In (F), immunodetection was made with anti-VPS35 and anti-VPS26A antibodies. In both panels, anti-α-Tubulin was used as a loading control.

Data information: In (A), (C-D) and (F), images are representative of three independent experiments. In (B) and (E), data are pooled from three independent experiments. Data are presented as median and quartiles. **P < 0.01, ***P < 0.001 (Mann-Whitney test). Source data are available online for this figure.

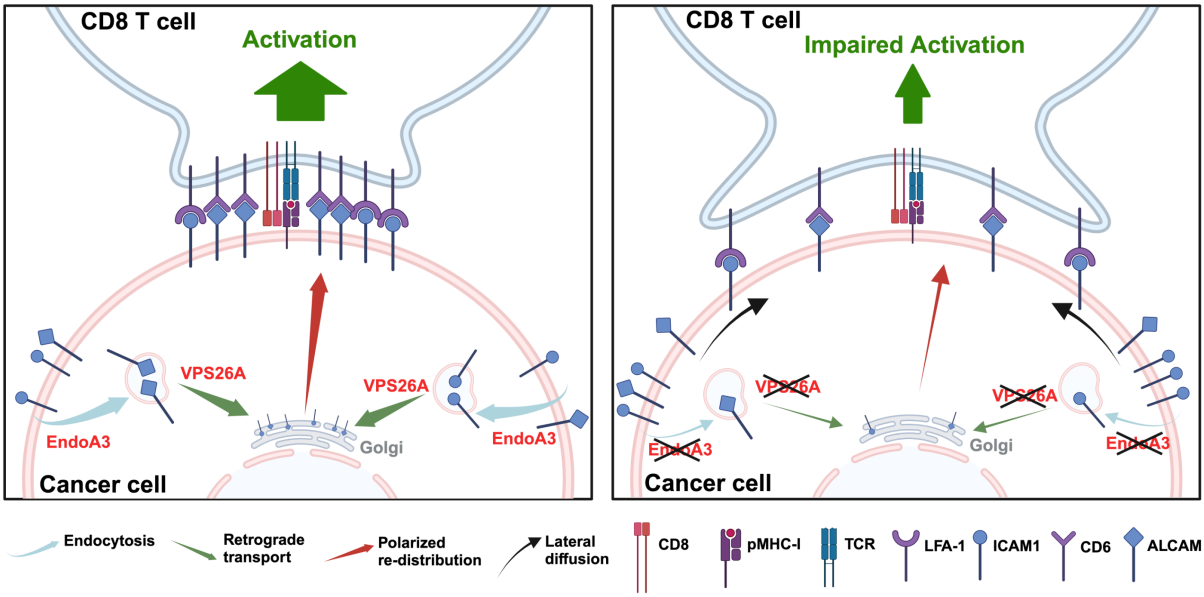

Figure 6. Model depicting how unconventional EndoA3-mediated endocytosis and retrograde transport in cancer cells promote CD8 T cell activation

Immune synapse components ALCAM and ICAM1 are endocytosed into cancer cells through EndoA3-mediated CIE and are subsequently transported to the *TGN* in a retromer-dependent retrograde manner. Upon immune synapse formation, immune synapse components, such as ALCAM and ICAM1, are efficiently recruited to the contact area with CD8 T cells, likely from the *TGN* by polarized re-distribution, which can stabilize the immune synapse and promote CD8 T cell activation (left). Consequently, disruption of EndoA3-mediated CIE or retromer-dependent retrograde transport in cancer cells impair the efficient recruitment of immune synapse components to the contact area with CD8 T cells. In this situation, CD8 T cells expand their contact areas with cancer cells to try to compensate the loss of immune synapse components. The compensation is insufficient, which ultimately results in impaired T cell activation (right).

Materials and Methods

Cell culture

Wild-type HeLa cell line was from ATCC®. GalT-GFP-SNAP-expressing HeLa cell line was generated in a previous study (Shi *et al*, 2012). EndoA3-GFP-expressing HeLa cell line was previously generated by our lab (Renard *et al.*, 2020). HLA-A*68012-expressing HeLa cell line was generated for the current study. Wild-type LB33-MEL cell line was derived from a melanoma patient in 1988 in de Duve Institute (Lehmann *et al.*, 1995). EndoA3-GFP-expressing and GalT-GFP-SNAP-expressing LB33-MEL cell lines were generated for the current study. Anti-MUM-3 CD8 T cells were derived from the same melanoma patient in 1990 in de Duve Institute (Lehmann *et al.*, 1995). Epstein-Barr virus transformed B cells from cancer patient LG-2 (LG-2 EBV) were obtained as described (Degiovanni *et al*, 1988).

Wild-type HeLa cells were cultured at 37°C under 5% CO_2 in high glucose DMEM (Gibco, 41966-029) supplemented with 10% FBS (Dulis, 500105N1N), 100 U/mL penicillin and 100 µg/mL streptomycin (Penicillin-Streptomycin, Gibco, 15140-122). EndoA3-GFP-expressing, GalT-GFP-SNAP-expressing, and HLA-A*68012-expressing HeLa cells were cultured at 37°C under 5% CO_2 in high glucose DMEM (Gibco, 41966-029) supplemented with 10% FBS, 100 U/mL penicillin, 100 µg/mL streptomycin, and 0.5 mg/mL G418 (Roche, 108321-42-2). WT LB33-MEL cells were cultured at 37°C under 5% CO_2 in IMDM (Gibco, 12440-053) supplemented with 10% FBS, 100 U/mL penicillin, 100 µg/mL streptomycin, 1.5 mM GlutaMAX I (Gibco, 35050-038), and 0.05 mM β-mercaptoethanol (Gibco, 21985-023). Empty plasmid stably transfected (Φ), EndoA3-GFP-expressing, and GalT-GFP-SNAP-expressing LB33-MEL cells were cultured in the same medium as WT LB33-MEL cells but supplemented with 0.7 mg/mL G418 (Roche, 108321-42-2). Anti-MUM-3 CD8 T cells were freshly thawed from cryovials and cultured at 37°C under 5% CO_2 in IMDM (Gibco, 12440-053) supplemented with 10% HS (Ludwig Institute for Cancer Research (LICR), Brussels Branch), 100 U/mL penicillin, 100 µg/mL streptomycin, 1.5 mM GlutaMAX I, and extra 5 U/mL DNase I (STEMCELL Tochnologies, 07469) and 50 U/mL IL-2 (PROLEUKIN®, CNK 1185-958) for at least 4 h before usage. For culture, T cells were maintained with the same medium, but without DNase I. LG-2 EBV cells were cultured at 37°C under 8% CO_2 in IMDM (Gibco, 21980-032) supplemented with 10% FBS (Gibco, A5256701), 100 U/mL penicillin, 100 µg/mL streptomycin and 1.5 mM GlutaMAX I (Gibco, 35050-038).

DNA constructs and transfection

Plasmids used in this study are listed below:

Protein	Backbone	Tag	Source
EndoA3	pIRESneo2	GFP	F. Tyckaert, LIBST, BE
/	pIRESneo3	/	Clontech
ICAM1	pLV-mScarlet	mScarlet	J. D. Van Buul, Amsterdam UMC, NL
ICAM1	pEGFP-N1	EGFP	Generated in the lab for this study
GalT-GFP-SNAP	pSNAP-tag	GFP	L. Johannes, Institut Curie, FR
/	pEGFP-N1	EGFP	Clontech
HLA-A*68012	pcDNA3	/	P. van der Bruggen, de Duve Institute, BE

C-terminally EGFP-tagged ICAM1 expression plasmid was generated in the current study for live-cell imaging. ICAM1 sequence was first amplified by PCR from the aforementioned mScarlet-tagged ICAM1 expression plasmid, and then inserted into the pEGFP-N1 vector by Gibson Assembly® (New England Biolabs). To do so, the vector was linearized with the restriction enzyme EcoR I, and corresponding overlapping sequences were added to both ends of ICAM1 inserts by PCR (forward primer: 5'-CGAGCTCAAGCTTCGATGGCTCCCAGCAGC-3'; reverse primer: 5'-TACCGTCGACTGCAGGGGAGGCGTGGCTTG-3'). The Gibson assembly product was then amplified in *E. coli* DH10B strain and validated by sequencing.

For immunofluorescence and live-cell imaging experiments, plasmids were transfected with FuGene HD (Promega), according to the manufacturer's instructions. Cells were used for experiments 16–24 h after transfection.

To generate the stable HLA-A*68012-expressing HeLa cell line, the pcDNA3-HLA-A*68012 plasmid was transfected into wild-type HeLa cells by nucleofection (Amaxa Nucleofector 2b, Lonza) according to the built-in protocol. Transfected cells were cultured for 2 days. A selection pressure was then imposed by supplementing the culture medium with 1 mg/mL G418 for 7 days. Cells were then harvested and maintained with 0.5 mg/mL G418 in the culture medium.

For the generation of different stable LB33-MEL cell lines, 300,000 wild-type LB33-MEL cells were seeded in 2 mL culture medium. 4 µg of corresponding plasmid (pIRESneo3 for LB33-MEL Φ generation, pIRESneo2-EndoA3-GFP-FKBP for EndoA3-GFP-expressing LB33-MEL generation, and pGalT-GFP-SNAP-tag for GalT-GFP-SNAP-expressing LB33-MEL generation) were added to 200 µL of Opti-MEM (Gibco), followed by addition of 24 µL of FuGENE HD (Promega) and gentle mixing. The mix was incubated for 15 min at room temperature, and then added to the cells. After 2 days of culture, transfected cells were selected by supplementing the culture medium with 0.7 mg/mL G418 for 7-15 days. Cell sorting based on GFP fluorescence was then conducted with the FACSAria flow cytometer (BD Biosciences) to yield a 100% positive stable EndoA3-GFP-expressing LB33-MEL cell line. For LB33-MEL cells transfected with GalT-GFP-SNAP-expressing plasmid, the homogeneity of cells was checked on a FACSVerse at the end of selection, and all cells were GFP-positive. Stable LB33-MEL Φ, EndoA3-GFP-

expressing LB33-MEL and GalT-GFP-SNAP-expressing LB33-MEL cell lines were then maintained with continuous presence of 0.7 mg/mL G418 in the culture medium.

RNA interference

siRNAs were used to knock down target molecules in HeLa and LB33-MEL cell lines at a total final concentration of 40nM. For HeLa cells, 150,000 cells were seeded per well of a 6-well plate for each siRNA condition, and siRNA transfection was conducted with 1 µL Lipofectamine RNAiMAX (ThermoFisher). For LB33-MEL cells, 200,000 cells were seeded per well of a 6-well plate for each siRNA condition, and siRNA transfection was conducted with 2 µL Lipofectamine RNAiMAX (ThermoFisher). All experiments were done 72 h after siRNA transfection. All siRNAs were purchased from QIAGEN, and their sequences are listed as follows:

Name	Reference	Sequence
Hs_SH3GL3_5	SI04170376	CCAGACGAGAATACAAGCCAA
Hs_SH3GL3_6	SI04176529	CCAGACGAAGAAGTCAGACAA
Hs_VPS26A_1	SI03122273	AAAGGTAAACCTAGCCTTTAA
Hs_VPS26A_2	SI04197914	TGCCACCTATCCTGATGTTAA
Hs_VPS35_7	SI04287605	CAGAATTGCCCTTAAGACTTT
Hs_VPS35_8	SI04316914	TTGCTGCATCCAAACTTCTAA
AllStars Negative Control	SI03650318	NA

T cell proliferation assay

HLA-A*68012 expressing HeLa cells were detached with PBS-EDTA 2 mM and resuspended to 1,000,000 cells/mL in the culture medium supplemented with or without MUM-3 peptide (EAFIQPITR) at 300 ng/mL. Then, HeLa cells and LG-2 EBV feeder cells were γ-irradiated for 45min (100Gy), washed, and maintained in T cell culture medium until the initiation of co-culture with T cells. The anti-MUM-3 CD8 T cells were thawed the day before and were harvested, washed, and resuspended in complete T cell culture medium with 0.5 µM CMFDA (Invitrogen™, C2925) for 20 min at 37°C. T cells were then washed and resuspended to 300,000 cells/mL in T cell medium supplemented with 50 U/mL IL-2. In an ultra-low attachment round bottom 96-well plate (Corning® Costar®, CLS7007), 30,000 anti-MUM-3 CD8 T cells were seeded with 10,000 HeLa cells and 90,000 γ-irradiated LG-2 EBV feeder cells. The plate was quickly centrifuged and then incubated for 4 days at 37°C with 5% CO_2. Cells were then transferred on ice for antibody staining and flow cytometry analysis.

Flow cytometry data were acquired with a LSR Fortessa (BD Biosciences) and were analyzed using FlowJo (v10.8.1) software.

IFNγ secretion assay

CD8 T cells were thawed and cultured as described above. siRNA transfected LB33-MEL cells were harvested 72 h after the siRNA transfection and were resuspended to 300,000

cells/mL in T cell medium. CD8 T cells were then washed and resuspended to 300,000 cells/mL in fresh T cell medium supplemented with 50 U/mL IL-2. 100 µL of LB33-MEL cells and 100 µL of T cells were pooled together in a 96-well plate and were co-cultured for 20 h at 37°C under 5% CO_2. A technical triplicate was made for each siRNA condition. The supernatant was collected the next day for ELISA analysis.

ELISA plate was coated with 50 µL IFNγ monoclonal coating antibody solution (Invitrogen, AHC4432; 1:250 dilution in PBS) in each well and was incubated at 4°C overnight. On the next day, two standard IFNγ concentration ladders were prepared: 1:2 dilutions for 7 successive times with T cell medium in 96-well plate (original concentration of 10,000 pg/mL; the last well contains only medium). The ELISA plate was washed with washing buffer (0.154 M NaCl solution with 0.1% Tween-20) twice and with water once to remove unbound antibody. 50 µL of supernatant and standard IFNγ ladders were then added to the ELISA plate, followed by the addition of 50 µL IFNγ monoclonal detecting antibody solution (biotin conjugated; Invitrogen, AHC4539; 1:1000 dilution in T cell medium) into each well. The plate was incubated on a shaker at 37°C for 2 h, and then was washed again. 50 µL of Streptavidin-Peroxydase solution (Sigma, S5512; 1:1000 dilution in PBS containing 0.5% bovine serum albumin) was added to each well and the plate was again incubated at 37°C for 30 min. Then, the plate was washed and 100 µL of 1-Step Ultra TMB-ELISA Substrate Solution (ThermoFisher, 34028) was added to each well. When the blue color of TMB stopped getting darker, 20 µL of sulfuric acid (1 M) was added to each well to stop the reaction (the blue color turned yellow). The absorbance of substrate solution at 450 nm was then measured with an ELISA Analyzer (Bio-Rad Microplate Reader) and the IFNγ concentration was determined.

Quantification of intracellular cytokines in CD8 T cells

CD8 T cells were thawed and cultured as described above. LB33-MEL cells were harvested 72 h after siRNA transfection and resuspended to 100,000 cells/mL in T cell medium. T cells were then washed and resuspended to 100,000 cells/mL in fresh T cell medium supplemented with 50 U/mL IL-2. 100 µL LB33-MEL cells and 100 µL T cells were pooled together in a 96-well “U” bottom plate and were co-cultured at 37°C under 5% CO_2 for 1 h. Then, Brefeldin A (Sigma, B7651-5MG) was added to each well at a final concentration of 5 µg/mL. Co-culture continued for another 3 h, after which cells were transferred to a 96-well “V” bottom plate and washed with 150 µL/well of staining buffer (PBS with 1mM EDTA and 1% HS). The plate was quickly spun at 400×g for 3 min and supernatant was removed. 50 µL of extracellular staining antibody solution for CD8 and viability marker prepared with staining buffer were added to each well and mixed. The plate was then maintained at 4°C for 20 min in the dark. Afterwards, cells were washed with 150 µL/well PBS and resuspended in 100 µL/well of 1% paraformaldehyde (PFA) for 10 min at room temperature. Cells were then washed with PBS again and resuspended in 100 µL PBS containing 1 mM EDTA, 1% HS, and 0.1% saponin. After 10 min incubation at room temperature, cells were centrifuged, and supernatant was removed. 50 µL of intracellular staining antibody solution for cytokines prepared with the same buffer was added to each well, and the plate was incubated in the dark for 30 min at room

temperature. Finally, cells were washed and resuspended in 250 µL 1% PFA for flow cytometry analysis.

Flow cytometry data were acquired with a FACSVerse (BD Biosciences) and were analyzed using FlowJo (v10.8.1) software.

Western blotting

Cell lysates were prepared with 200,000 cells and 50 µL of sample buffer (62.5 mM Tris-HCl pH 6.8, 2% sodium dodecyl sulfate (SDS), 5% glycerol, 2.5% β-mercaptoethanol, 0.005% blue bromophenol). Lysate samples were boiled at 95°C for 10 min before loading onto 4–15% Mini-PROTEAN® TGX™ precast protein gels (Bio-Rad, 4561084), as well as prestained protein standard. For the SNAP-Tag-based retrograde transport assay (see below), HiMark™ Pre-stained Protein Standard (Invitrogen, LC5699) was used; for all the other western blots, Broad Range (10-250 kDa) Color Prestained Protein Standard (New England Biolabs, P7719S) was used. After electrophoresis, proteins were transferred onto a PVDF membrane (pre-activated with methanol for 1 min; Millipore, IPFL85R) using a wet transferring system. The membrane was then blocked in 5%-milk PBS-T (phosphate-buffered saline, 0.1% Tween-20) for 1h at room temperature, then stirred overnight at 4°C with primary antibody in the same solution. The next day, the membrane was incubated with corresponding horseradish peroxidase (HRP) conjugated secondary antibodies for 1h at room temperature. Chemiluminescent (ECL) substrate (SuperSignal™ West Femto Maximum Sensitivity Substrate, ThermoFisher, 34096, or SuperSignal™ West Pico PLUS Chemiluminescent Substrate, ThermoFisher, 34580) was used for image exposure with an Amersham ImageQuant™ 800 machine (Cytiva). Images were processed and quantified with ImageJ v2.14.0/1.54f (NIH) software.

SNAP-Tag-based retrograde transport assay

First, anti-ALCAM (Bio-Rad, MCA1926) and anti-ICAM1 (Bio-Rad, MCA1615) antibodies were labeled with benzylguanine (BG) by incubating them overnight at 4°C with a threefold molar excess of BG-GLA-NHS reagent (New England Biolabs, S9151S; prepared in anhydrous DMSO). The reaction was neutralized with 20 mM Tris (pH 7.4) for 10 min at 21°C. Free BG-GLA-NHS was eliminated by applying labelled antibodies on spin desalting columns with a 7 kDa cutoff (ThermoFisher, 89849), according to manufacturer's instructions. Then, retrograde transport assays were conducted according to previously published protocols (Shafaq-Zadah *et al.*, 2021).

Colocalization and uptake experiments

LB33-MEL cells were cultured on coverslips in 4-well plates to reach sub-confluence on the day of the experiment. Cells were pre-incubated in fresh serum-containing medium for 30 min at 37°C just before the experiment, then were incubated with anti-ALCAM antibody (Biolegend, 343902)-containing pre-warmed medium (5 µg/mL) for 15 min at 37°C to allow for endocytosis. For colocalization experiments, cells were quickly washed at 37°C with pre-warmed PBS and were subsequently fixed with pre-warmed 4% PFA for

20 min at 37°C in order to preserve the integrity of cellular structures and protein distribution. For uptake experiments, endocytosis was stopped on ice, and unbound antibodies were removed by extensive washes with ice-cold PBS++ (PBS supplemented with 0.4 mM $MgCl_2$ and 0.9 mM $CaCl_2$). Residual cell surface-accessible anti-ALCAM antibodies were stripped by two 5 s acid washes on ice (200 mM acetic acid, pH 2.5, 300 mM NaCl, 5 mM NaCl, 1 mM $CaCl_2$, and 1 mM $MgCl_2$). After neutralization by extensive washes with ice-cold PBS++, cells were fixed with 4% PFA for 10 min on ice, followed by another 10 min at room temperature. For both experiments, after quenching with 50 mM NH_4Cl for at least 5 min, cells were permeabilized with 0.02% saponin in PBS containing 0.2% bovine serum albumin for 30 min at room temperature. After incubation with secondary antibodies in the same permeabilization solution for 30 min, samples were mounted with Fluoromount G (Invitrogen). Images were taken with a Zeiss LSM900 microscope equipped with an Airyscan detector and a Plan Apo 63× numerical aperture (NA) 1.4 oil immersion objective. For colocalization experiments, Airyscan mode was applied. Pixel size: 0.04 micron. For uptake experiments, confocal mode was used. Pixel size: 0.07 micron. Microscope software: Zen blue (v3.3; Zeiss).

Conjugate formation for confocal fixed sample imaging

For conjugate formation between adherent HLA-A*68012-expressing HeLa cells and anti-MUM-3 CD8 T cells (Fig 4B, EV4C), HeLa cells were cultured on coverslips and transiently transfected with ICAM1-mScarlet expression plasmid 16-24h before the experiment. HeLa cells were first incubated in 300 ng/mL MUM-3 peptide-containing culture medium for 45 min at 37°C and were then washed extensively with T cell culture medium to remove residual unbound peptide. T cells were freshly thawed as described above and resuspended to 500,000 cells/mL with T cell culture medium supplemented with 50 U/mL IL-2. Then, 250,000 T cells were added to HeLa cells and the pool was incubated for 20 min at 37°C. Cells were then fixed at room temperature for 20 min by adding PFA directly to the culture medium to reach a final concentration of 4%.

For conjugate formation between suspended HLA-A*68012-expressing HeLa cells and anti-MUM-3 CD8 T cells (Fig 4C, EV4D), HeLa cells were cultured in 6-well plates and transfected with negative control siRNAs or siRNAs targeting EndoA3 72h in advance and with plasmid expressing ICAM1-mScarlet 16-24h in advance. HeLa cells were detached with PBS-EDTA 4 mM, resuspended to 1,000,000 cells/mL in culture medium containing 300 ng/mL MUM-3 peptide and incubated for 45 min at room temperature. Then, HeLa cells were extensively washed with T cell culture medium, and finally resuspended to 1,000,000 cells/mL with T cell culture medium supplemented with 50 U/mL IL-2. T cells were freshly thawed as described above and resuspended to 1,000,000 cells/mL with T cell culture medium supplemented with 50 U/mL IL-2. Subsequently, 250,000 HeLa cells and 250,000 T cells were pooled together and further co-cultured on coverslips for 20 min at 37°C. Of note, coverslips were pre-coated with poly-L-lysine (Sigma-Aldrich, P4832) according to manufacturer's instructions to stabilize conjugates. Cells were then fixed at room temperature for 20 min by adding PFA directly to the culture medium to reach a final concentration of 4%.

For conjugate formation between suspended EndoA3-GFP-expressing LB33-MEL cells and anti-MUM-3 CD8 T cells (Fig 5, EV5), LB33-MEL cells were transfected with negative control siRNAs or siRNAs targeting EndoA3 or VPS26A 72h in advance. LB33-MEL cells were detached with 0.05% Trypsin-EDTA (Gibco, 25300-054) and resuspended to 1,000,000 cells/mL with T cell culture medium supplemented with 50 U/mL IL-2. T cells were freshly thawed as described above and resuspended to 1,000,000 cells/mL with T cell culture medium supplemented with 50 U/mL IL-2. Then, 250,000 LB33-MEL cells and 250,000 T cells were pooled together and were co-cultured on poly-L-lysine pre-coated coverslips for 20 min at 37°C. Cells were then fixed at room temperature for 20 min by adding PFA directly to the culture medium to reach a final concentration of 4%.

After fixation with PFA and quenching with 50 mM NH_4Cl for at least 5 min, cells were permeabilized with 0.02% saponin in PBS containing 0.2% bovine serum albumin for 30 min, both at room temperature. Then, cells were successively incubated with primary and secondary antibodies in the same PBS-saponin solution for 30 min and mounted with Fluoromount G (Invitrogen). Images were taken with Zeiss LSM900 microscope equipped with an Airyscan detector and a Plan Apo 63× numerical aperture (NA) 1.4 oil immersion objective. For the ICAM1 recruitment experiment (Fig 4B, EV4C) and immune synapse morphology experiment (Fig 5, EV5), z-stack was used. z-stack interval: 0.15 micron. For all images, Airyscan mode was applied. Pixel size: 0.04 micron. Microscope software: Zen blue (v3.3; Zeiss).

Conjugate formation for confocal live-cell imaging

HLA-A*68012-expressing HeLa cells were seeded in 24-well glass bottom plates (Greiner, 662892) and transfected with ICAM1-EGFP expression plasmid 16-24 h in advance. HeLa cells were first incubated in MUM-3 peptide-containing (300 ng/mL) culture medium for 45 min at 37°C and then washed extensively with T cell culture medium to remove residual unbound peptide. Anti-MUM-3 CD8 T cells were freshly thawed as described above and stained with Orange CellMask™ Plasma Membrane Stain (Invitrogen, C10045; 1:1000 dilution in T cell culture medium) for 10 min at 37°C, washed with culture medium, and resuspended to 500,000 cells/mL in T cell culture medium supplemented with 50 U/mL IL-2. 250,000 T cells were added to each well containing HeLa cells and live-cell imaging was started immediately after. Live-cell imaging was performed at 5% CO_2 and 37°C on a Zeiss LSM900 confocal microscope equipped with an Airyscan detector, an α Plan Apo 63× numerical aperture (NA) 1.4 oil immersion objective and a stage-top incubator. Microscope was controlled by software Zen blue (v3.3; Zeiss). Laser focus was maintained with definite focus 2. Airyscan mode was applied. Time interval between each frame: 6.5 s. Pixel size: 0.04 micron.

TIRF live-cell imaging

EndoA3-GFP-expressing HeLa/LB33-MEL cells were cultured on a 35 mm imaging dish with a glass bottom and low walls (ibidi, μ-Dish 35 mm, low, 80137) and transfected with ICAM1-mScarlet expression plasmid 16-24 h in advance. Live-cell imaging was conducted under 5% CO_2 and 37°C with Zeiss Axio Observer 7 microscope equipped

with an iLas azimuthal TIRF module (Gattaca Systems), an α Plan-Apo 100× NA 1.46 oil immersion objective, an sCMOS Prime BSI Express camera (Photometrics) and a stage-top incubator (Tokai Hit). Microscope was controlled by Metamorph® software (v7.10.4.407; Molecular Devices). Laser focus was maintained with definite focus 3. Time interval between each frame: 1 s. Pixel size: 0.065 micron.

Microscope image analyses and quantifications

Airyscan image processing was performed with Zen blue (v3.3; Zeiss). Images were quantified with (Fiji Is Just) ImageJ v2.14.0/1.54f (NIH) software as follows.

For CD166 uptake experiments, images were quantified using Icy v2.4.2.0 (Institut Pasteur) software. Briefly, regions of interest (ROIs) were drawn manually around each cell. Within each ROI, bright spots corresponding to endocytic structures were automatically detected over dark background using the "Spot Detector" plugin. The plugin performs image denoising by computing wavelet adaptive threshold (WAT) on the union of all ROIs present in an image. This automatic thresholding was then manually adjusted, depending on the size of the spots. For each independent experiment, scale 2 was chosen and sensitivity was adjusted empirically. In addition, a size filter was added to discard spots smaller than 2 pixels. After processing, an excel file containing the fluorescence intensity of each endocytic structure was generated. The sum intensity of endocytic structures in each cell was calculated, then data were first adjusted according to the surface level of CD166 detected by flow cytometry in each experimental condition and were finally normalized to the control condition (set as 100%) for statistical analysis.

For conjugate formation experiments with HeLa cells to detect ICAM1 recruitment to the vicinity of CD8 T cells, masks were automatically generated for each image according to phalloidin staining by using Cellpose v3.0.7 software (Stringer & Pachitariu, 2024). First, an RGB format 512 × 512-pixel image of the phalloidin channel was generated from Fiji (ImageJ v2.14.0/1.54f) for each image and was imported to Cellpose. Segmentation of each cell was automatically performed using "cyto3" model with diameter (pixels) set as 40 for all independent repeats and was then exported as a mask. The mask was then imported into Fiji and re-scaled to the real size of the original image. Wand tool was used to select ROI corresponding to single cells. In each ROI, the raw integrated density (RawIntDen) of ICAM1 signal was measured. Then, the ICAM1 recruitment ratio in the vicinity of the T cell was calculated as the ratio between the ICAM1 signal in the T cell ROI and the total ICAM1 signal in the ROIs of the T cell and the adjacent HeLa cell: "RawIntDen of ICAM1 signal in T cell ROI/(RawIntDen of ICAM1 signal in T cell ROI + RawIntDen of ICAM1 signal in HeLa cell ROI)". Data were normalized to control condition (set as 100%) for each independent repeat and were then pooled together for statistical analysis.

For conjugate formation experiments to measure the size of immune synapses, z-stack images (z-stack interval: 0.15 micron) for each conjugate were imported to Fiji. The contact region between a CD8 T cell and an LB33-MEL cell was delineated by "freehand line" tool manually, and then the length of the line was measured for each z-stack. The

largest value was picked out from all z-stacks and was considered as the size of this immune synapse. All data from three independent repeats were then pooled together for statistical analysis.

Statistical analyses

Statistical analyses were performed with GraphPad Prism v10.1.0. D'Agostino–Pearson omnibus normality test was used to check the normality of datasets. If data passed the normality test, parametric tests were used, and data were plotted on graphs as mean ± SEM as error bars. If data did not pass the normality test, nonparametric tests were used, and data were plotted on graphs as median and quartiles. Details on the parametric and nonparametric tests used for each analysis are indicated in figure legends. Significance of comparison is represented on the graphs by asterisks.

Antibodies and reagents

Product	Reference	Application	Dilution
PE anti-human CD166 antibody	Biolegend, 343904	FACS	1:1000
APC anti-human CD54 antibody	BD Pharmingen, 561899	FACS	1:60
APC anti-HLA-A2, A28 antibody	Miltenyi Biotec, 130-099-582	FACS	1:300
Viability Dye eFluor 780	Invitrogen, 65-0865-14	FACS	1:1000
PerCP-Cy5.5 anti-human CD8 antibody	BD Pharmingen, 624060	FACS	1:100
APC anti-human IL-2 antibody	Biolegend, 500310	FACS	1:25
BV421 anti-human TNF-α antibody	Biolegend, 502932	FACS	1:100
PE anti-human IFNγ antibody	BD Pharmingen, 554701	FACS	1:200
Biotin anti-human HLA-A2 Antibody	Biolegend, 343322	FACS	1:400
CMFDA	Invitrogen, C2925	FACS	0.5 μM
Anti-IFNγ coating antibody	Invitrogen, AHC4432	ELISA	1:250
Biotin anti-IFNγ detecting antibody	Invitrogen, AHC4539	ELISA	1:1000
Streptavidin−Peroxidase	Sigma-Aldrich, S5512	ELISA	1:1000
1-Step Ultra TMB-ELISA Substrate	ThermoFisher, 34028	ELISA	100 μL
Anti-SH3GL3/Endophilin-A3 antibody	Sigma-Aldrich, HPA039381	WB	1:1000
Anti-α-tubulin antibody	Sigma-Aldrich, T5168	WB	1:10000
Anti-VPS26A antibody	abcam, ab23892	WB	1:1000
Anti-VPS35 antibody	abcam, ab10099	WB	1:500
HRP conjugated anti-mouse antibody	Agilent Technologies, P044701-2	WB	1:5000
HRP conjugated anti-rabbit antibody	Agilent Technologies, P044801-2	WB	1:5000
HRP conjugated anti-goat antibody	Santa Cruz Biotechnology, sc-2354	WB	1:1000
Anti-SNAP-tag® antibody	New England Biolabs, P9310S	WB	1:1000
Anti-CD166 antibody	Bio-Rad, MCA1926	SNAP-Tag	10 μg/mL
Anti-CD54 antibody	Bio-Rad, MCA1615	SNAP-Tag	10 μg/mL
SNAP-Cell® Block	New England Biolabs, S9106S	SNAP-Tag	1:200
Anti-CD166 antibody	Biolegend, 343902	IF	1:100
Anti-CD45 antibody	Santa Cruz Biotechnology, sc-1178	IF	1:100
SNAP-Cell® TMR-Star	New England Biolabs, S9105S	IF	1:200
Anti-GM130 antibody	Biolegend, 937002	IF	1:200
Alexa Fluor™ 488 Phalloidin	Invitrogen, A12379	IF	1:200
Alexa Fluor™ 568 Phalloidin	Invitrogen, A12380	IF	1:200
Alexa Fluor™ 488 anti-Rabbit IgG	Invitrogen, A11008	IF	1:200
Alexa Fluor™ 568 anti-Mouse IgG	Invitrogen, A11031	IF	1:200
Alexa Fluor™ 633 anti-Mouse IgG	Invitrogen, A21050	IF	1:200

CellMask™ Plasma Membrane Stain	Invitrogen, C10045	IF	1:1000
DAPI	Sigma-Aldrich, D9542	IF	1:10000
Poly-L-lysine	Sigma-Aldrich, P4832	IF	NA

Acknowledgements:

We thank J.D. van Buul (Amsterdam UMC, Netherlands) for kindly providing aforementioned plasmid. We thank E. Rigaux, F. Tyckaert, C. Wildmann, C. Duhamel, S. Meurant, A. Fattaccioli, S. Burteau and C. Demazy for their support and technical help in experiments. We greatly thank Morph-Im platform of UNamur and flow cytometry & cell sorting platform (CYTF) from de Duve Institute of UCLouvain for giving access to advanced microscopy and flow cytometry technologies, respectively.

S.X. is supported by a PhD fellowship from FSR (Fond Spécial de Recherche) of UNamur and UCLouvain. T.H. is a postdoctoral research fellow of the Fonds de la Recherche Scientifique (FNRS, Belgium). L.J. is supported by Mizutani Foundation for Glycosciences (reference n° 200014), Agence National de la Recherche (ANR-20-CE15-0009-01, ANR-22-CE11-0030-03, France), Fondation pour la Recherche Médicale (EQU202103012926, France) and an ERC Proof of Concept (project 101062030). P.V.D.B. and T.H. were supported by de Duve Institute (Belgium) and Université Catholique de Louvain (Belgium). P.M. is supported by a PDR (T.0163.21) and CDR (J.0127.23) from the Fonds de la Recherche Scientifique (FNRS, Belgium). H.-F.R. is supported by a Start-Up Grant Collen-Francqui from Francqui Foundation (Belgium), an Incentive Grant for Scientific Research (MIS-F.4540.21) and a Research Credit (CDR-J.0176.24) from the Fonds de la Recherche Scientifique (FNRS, Belgium), and a research grant from NARILIS institute (UNamur).

References:

Arai F, Ohneda O, Miyamoto T, Zhang XQ, Suda T (2002) Mesenchymal stem cells in perichondrium express activated leukocyte cell adhesion molecule and participate in bone marrow formation. *J Exp Med* 195: 1549-1563

Aruffo A, Bowen MA, Patel DD, Haynes BF, Starling GC, Gebe JA, Bajorath J (1997) CD6-ligand interactions: a paradigm for SRCR domain function? *Immunol Today* 18: 498-504

Baurain JF, Colau D, van Baren N, Landry C, Martelange V, Vikkula M, Boon T, Coulie PG (2000) High frequency of autologous anti-melanoma CTL directed against an antigen generated by a point mutation in a new helicase gene. *J Immunol* 164: 6057-6066

Boucrot E, Ferreira AP, Almeida-Souza L, Debard S, Vallis Y, Howard G, Bertot L, Sauvonnet N, McMahon HT (2015) Endophilin marks and controls a clathrin-independent endocytic pathway. *Nature* 517: 460-465

Bowen MA, Patel DD, Li X, Modrell B, Malacko AR, Wang WC, Marquardt H, Neubauer M, Pesando JM, Francke U *et al* (1995) Cloning, mapping, and characterization of activated leukocyte-cell adhesion molecule (ALCAM), a CD6 ligand. *J Exp Med* 181: 2213-2220

Bugarcic A, Zhe Y, Kerr MC, Griffin J, Collins BM, Teasdale RD (2011) Vps26A and Vps26B subunits define distinct retromer complexes. *Traffic* 12: 1759-1773

Carpier JM, Zucchetti AE, Bataille L, Dogniaux S, Shafaq-Zadah M, Bardin S, Lucchino M, Maurin M, Joannas LD, Magalhaes JG *et al* (2018) Rab6-dependent retrograde traffic of LAT controls immune synapse formation and T cell activation. *J Exp Med* 215: 1245-1265

Chen KE, Healy MD, Collins BM (2019) Towards a molecular understanding of endosomal trafficking by Retromer and Retriever. *Traffic* 20: 465-478

Deeths MJ, Mescher MF (1999) ICAM-1 and B7-1 provide similar but distinct costimulation for CD8+ T cells, while CD4+ T cells are poorly costimulated by ICAM-1. *European Journal of Immunology* 29: 45-53

Degiovanni G, Lahaye T, Hérin M, Hainaut P, Boon T (1988) Antigenic heterogeneity of a human melanoma tumor detected by autologous CTL clones. *European Journal of Immunology* 18: 671-676

Dieckmann NM, Frazer GL, Asano Y, Stinchcombe JC, Griffiths GM (2016) The cytotoxic T lymphocyte immune synapse at a glance. *J Cell Sci* 129: 2881-2886

Ferragut F, Vachetta VS, Troncoso MF, Rabinovich GA, Elola MT (2021) ALCAM/CD166: A pleiotropic mediator of cell adhesion, stemness and cancer progression. *Cytokine Growth Factor Rev* 61: 27-37

Fuse A, Furuya N, Kakuta S, Inose A, Sato M, Koike M, Saiki S, Hattori N (2015) VPS29-VPS35 intermediate of retromer is stable and may be involved in the retromer complex assembly process. *FEBS Lett* 589: 1430-1436

Gad H, Ringstad N, Löw P, Kjaerulff O, Gustafsson J, Wenk M, Di Paolo G, Nemoto Y, Crum J, Ellisman MH *et al* (2000) Fission and Uncoating of Synaptic Clathrin-Coated Vesicles Are Perturbed by Disruption of Interactions with the SH3 Domain of Endophilin. *Neuron* 27: 301-312

Gallop JL, Jao CC, Kent HM, Butler PJ, Evans PR, Langen R, McMahon HT (2006) Mechanism of endophilin N-BAR domain-mediated membrane curvature. *EMBO J* 25: 2898-2910

Genet G, Boye K, Mathivet T, Ola R, Zhang F, Dubrac A, Li J, Genet N, Henrique Geraldo L, Benedetti L *et al* (2019) Endophilin-A2 dependent VEGFR2 endocytosis promotes sprouting angiogenesis. *Nat Commun* 10: 2350

Giachino C, Lantelme E, Lanzetti L, Saccone S, Bella Valle G, Migone N (1997) A novel SH3-containing human gene family preferentially expressed in the central nervous system. *Genomics* 41: 427-434

Gimferrer I, Calvo M, Mittelbrunn M, Farnos M, Sarrias MR, Enrich C, Vives J, Sanchez-Madrid F, Lozano F (2004) Relevance of CD6-mediated interactions in T cell activation and proliferation. *J Immunol* 173: 2262-2270

Hassan NJ, Barclay AN, Brown MH (2004) Frontline: Optimal T cell activation requires the engagement of CD6 and CD166. *Eur J Immunol* 34: 930-940

Healy MD, McNally KE, Butkovic R, Chilton M, Kato K, Sacharz J, McConville C, Moody ERR, Shaw S, Planelles-Herrero VJ *et al* (2023) Structure of the endosomal Commander complex linked to Ritscher-Schinzel syndrome. *Cell* 186: 2219-2237 e2229

Hierro A, Rojas AL, Rojas R, Murthy N, Effantin G, Kajava AV, Steven AC, Bonifacino JS, Hurley JH (2007) Functional architecture of the retromer cargo-recognition complex. *Nature* 449: 1063-1067

Johannes L, Shafaq-Zadah M (2013) SNAP-tagging the retrograde route. *Methods Cell Biol* 118: 139-155

Johannes L, Wunder C, Shafaq-Zadah M (2016) Glycolipids and Lectins in Endocytic Uptake Processes. *J Mol Biol* 428: 4792-4818

Kaksonen M, Roux A (2018) Mechanisms of clathrin-mediated endocytosis. *Nat Rev Mol Cell Biol* 19: 313-326

Kamoun M, Kadin ME, Martin PJ, Nettleton J, Hansen JA (1981) A novel human T cell antigen preferentially expressed on mature T cells and shared by both well and poorly differentiated B cell leukemias and lymphomas. *J Immunol* 127: 987-991

Kerr MC, Bennetts JS, Simpson F, Thomas EC, Flegg C, Gleeson PA, Wicking C, Teasdale RD (2005) A novel mammalian retromer component, Vps26B. *Traffic* 6: 991-1001

Kjaerulff O, Brodin L, Jung A (2011) The structure and function of endophilin proteins. *Cell Biochem Biophys* 60: 137-154

Lakshminarayan R, Wunder C, Becken U, Howes MT, Benzing C, Arumugam S, Sales S, Ariotti N, Chambon V, Lamaze C *et al* (2014) Galectin-3 drives glycosphingolipid-dependent biogenesis of clathrin-independent carriers. *Nat Cell Biol* 16: 595-606

Lehmann F, Marchand M, Hainaut P, Pouillart P, Sastre X, Ikeda H, Boon T, Coulie PG (1995) Differences in the antigens recognized by cytolytic T cells on two successive metastases of a melanoma patient are consistent with immune selection. *Eur J Immunol* 25: 340-347

Lemaigre C, Ceuppens A, Valades-Cruz CA, Ledoux B, Vanbeneden B, Hassan M, Zetterberg FR, Nilsson UJ, Johannes L, Wunder C *et al* (2023) N-BAR and F-BAR proteins-endophilin-A3 and PSTPIP1-control clathrin-independent endocytosis of L1CAM. *Traffic* 24: 190-212

Mallam AL, Marcotte EM (2017) Systems-wide Studies Uncover Commander, a Multiprotein Complex Essential to Human Development. *Cell Syst* 4: 483-494

McNally KE, Faulkner R, Steinberg F, Gallon M, Ghai R, Pim D, Langton P, Pearson N, Danson CM, Nagele H *et al* (2017) Retriever is a multiprotein complex for retromer-independent endosomal cargo recycling. *Nat Cell Biol* 19: 1214-1225

Micheva KD, Kay BK, McPherson PS (1997) Synaptojanin forms two separate complexes in the nerve terminal. Interactions with endophilin and amphiphysin. *J Biol Chem* 272: 27239-27245

Milosevic I, Giovedi S, Lou X, Raimondi A, Collesi C, Shen H, Paradise S, O'Toole E, Ferguson S, Cremona O *et al* (2011) Recruitment of endophilin to clathrin-coated pit necks is required for efficient vesicle uncoating after fission. *Neuron* 72: 587-601

Moreno-Layseca P, Jantti NZ, Godbole R, Sommer C, Jacquemet G, Al-Akhrass H, Conway JRW, Kronqvist P, Kallionpaa RE, Oliveira-Ferrer L *et al* (2021) Cargo-specific recruitment in clathrin- and dynamin-independent endocytosis. *Nat Cell Biol* 23: 1073-1084

Peter BJ, Kent HM, Mills IG, Vallis Y, Butler PJG, Evans PR, McMahon HT (2004) BAR Domains as Sensors of Membrane Curvature: The Amphiphysin BAR Structure. *SCIENCE* 303

Petrelli A, Gilestro GF, Lanzardo S, Comoglio PM, Migone N, Giordano S (2002) The endophilin-CIN85-Cbl complex mediates ligand-dependent downregulation of c-Met. *Nature* 416: 187-190

Renard HF, Boucrot E (2021) Unconventional endocytic mechanisms. *Curr Opin Cell Biol* 71: 120-129

Renard HF, Simunovic M, Lemiere J, Boucrot E, Garcia-Castillo MD, Arumugam S, Chambon V, Lamaze C, Wunder C, Kenworthy AK *et al* (2015) Endophilin-A2 functions in membrane scission in clathrin-independent endocytosis. *Nature* 517: 493-496

Renard HF, Tyckaert F, Lo Giudice C, Hirsch T, Valades-Cruz CA, Lemaigre C, Shafaq-Zadah M, Wunder C, Wattiez R, Johannes L *et al* (2020) Endophilin-A3 and Galectin-8 control the clathrin-independent endocytosis of CD166. *Nat Commun* 11: 1457

Ringstad N, Nemoto Y, De Camilli P (1997) The SH3p4/Sh3p8/SH3p13 protein family: binding partners for synaptojanin and dynamin via a Grb2-like Src homology 3 domain. *Proc Natl Acad Sci U S A* 94: 8569-8574

Seaman MN (2004) Cargo-selective endosomal sorting for retrieval to the Golgi requires retromer. *J Cell Biol* 165: 111-122

Seaman MN, McCaffery JM, Emr SD (1998) A membrane coat complex essential for endosome-to-Golgi retrograde transport in yeast. *J Cell Biol* 142: 665-681

Shafaq-Zadah M, Dransart E, Johannes L (2020) Clathrin-independent endocytosis, retrograde trafficking, and cell polarity. *Curr Opin Cell Biol* 65: 112-121

Shafaq-Zadah M, Dransart E, Johannes L (2021) Quantitative Methods to Study Endocytosis and Retrograde Transport of Cargo Proteins. *Methods Mol Biol* 2233: 53-70

Shafaq-Zadah M, Gomes-Santos CS, Bardin S, Maiuri P, Maurin M, Iranzo J, Gautreau A, Lamaze C, Caswell P, Goud B *et al* (2016) Persistent cell migration and adhesion rely on retrograde transport of beta(1) integrin. *Nat Cell Biol* 18: 54-64

Shi G, Azoulay M, Dingli F, Lamaze C, Loew D, Florent JC, Johannes L (2012) SNAP-tag based proteomics approach for the study of the retrograde route. *Traffic* 13: 914-925

Simpson F, Hussain NK, Qualmann B, Kelly RB, Kay BK, McPherson PS, Schmid SL (1999) SH3-domain-containing proteins function at distinct steps in clathrin-coated vesicle formation. *Nat Cell Biol* 1: 119-124

Simunovic M, Manneville JB, Renard HF, Evergren E, Raghunathan K, Bhatia D, Kenworthy AK, Voth GA, Prost J, McMahon HT *et al* (2017) Friction Mediates Scission of Tubular Membranes Scaffolded by BAR Proteins. *Cell* 170: 172-184 e111

Singla A, Fedoseienko A, Giridharan SSP, Overlee BL, Lopez A, Jia D, Song J, Huff-Hardy K, Weisman L, Burstein E *et al* (2019) Endosomal PI(3)P regulation by the COMMD/CCDC22/CCDC93 (CCC) complex controls membrane protein recycling. *Nat Commun* 10: 4271

So CW, Sham MH, Chew SL, Cheung N, So CK, Chung SK, Caldas C, Wiedemann LM, Chan LC (2000) Expression and protein-binding studies of the EEN gene family, new interacting partners for dynamin, synaptojanin and huntingtin proteins. *Biochem J* 348 Pt 2: 447-458

Sonnichsen B, De Renzis S, Nielsen E, Rietdorf J, Zerial M (2000) Distinct membrane domains on endosomes in the recycling pathway visualized by multicolor imaging of Rab4, Rab5, and Rab11. *J Cell Biol* 149: 901-914

Soubeyran P, Kowanetz K, Szymkiewicz I, Langdon WY, Dikic I (2002) Cbl-CIN85-endophilin complex mediates ligand-induced downregulation of EGF receptors. *Nature* 416: 183-187

Sparks AB, Hoffman NG, McConnell SJ, Fowlkes DM, Kay BK (1996) Cloning of ligand targets: systematic isolation of SH3 domain-containing proteins. *Nat Biotechnol* 14: 741-744

Steinberg F, Gallon M, Winfield M, Thomas EC, Bell AJ, Heesom KJ, Tavare JM, Cullen PJ (2013) A global analysis of SNX27-retromer assembly and cargo specificity reveals a function in glucose and metal ion transport. *Nat Cell Biol* 15: 461-471

Stringer C, Pachitariu M (2024) Cellpose3: one-click image restoration for improved cellular segmentation. *bioRxiv*

Tang Y, Hu LA, Miller WE, Ringstad N, Hall RA, Pitcher JA, DeCamilli P, Lefkowitz RJ (1999) Identification of the endophilins (SH3p4/p8/p13) as novel binding partners for the beta1-adrenergic receptor. *Proc Natl Acad Sci U S A* 96: 12559-12564

Traub LM, Bonifacino JS (2013) Cargo recognition in clathrin-mediated endocytosis. *Cold Spring Harb Perspect Biol* 5: a016790

van der Sluijs P, Hull M, Webster P, Male P, Goud B, Mellman I (1992) The small GTP-binding protein rab4 controls an early sorting event on the endocytic pathway. *Cell* 70: 729-740

van Kempen LC, Nelissen JM, Degen WG, Torensma R, Weidle UH, Bloemers HP, Figdor CG, Swart GW (2001) Molecular basis for the homophilic activated leukocyte cell adhesion molecule (ALCAM)-ALCAM interaction. *J Biol Chem* 276: 25783-25790

Van Seventer GA, Shimizu Y, Horgan KJ, Shaw S (1990) The LFA-1 ligand ICAM-1 provides an important costimulatory signal for T cell receptor-mediated activation of resting T cells. *J Immunol* 144: 4579-4586

Wan C, Borgeson B, Phanse S, Tu F, Drew K, Clark G, Xiong X, Kagan O, Kwan J, Bezginov A *et al* (2015) Panorama of ancient metazoan macromolecular complexes. *Nature* 525: 339-344

Weichert W, Knosel T, Bellach J, Dietel M, Kristiansen G (2004) ALCAM/CD166 is overexpressed in colorectal carcinoma and correlates with shortened patient survival. *J Clin Pathol* 57: 1160-1164

Zimmerman AW, Joosten B, Torensma R, Parnes JR, van Leeuwen FN, Figdor CG (2006) Long-term engagement of CD6 and ALCAM is essential for T-cell proliferation induced by dendritic cells. *Blood* 107: 3212-3220

Zuckerman LA, Pullen L, Miller J (1998) Functional consequences of costimulation by ICAM-1 on IL-2 gene expression and T cell activation. *J Immunol* 160: 3259-3268